NASA TECHNICAL NOTE

NASA TN D-3214

NASA TN D-3214

RADAR CROSS SECTION AND OPTICAL RADIATION FROM THE TRAILBLAZER IIa 9° HALF-ANGLE BLUNT NOSE CONE DURING HYPERSONIC REENTRY

by Wayne L. Darnell

Langley Research Center
Langley Station, Hampton, Va.

NATIONAL AERONAUTICS AND SPACE ADMINISTRATION • WASHINGTON, D. C. • FEBRUARY 1966

NASA TN D-3214

RADAR CROSS SECTION AND OPTICAL RADIATION FROM THE TRAILBLAZER IIa 9° HALF-ANGLE BLUNT NOSE CONE DURING HYPERSONIC REENTRY

By Wayne L. Darnell

Langley Research Center
Langley Station, Hampton, Va.

NATIONAL AERONAUTICS AND SPACE ADMINISTRATION

For sale by the Clearinghouse for Federal Scientific and Technical Information
Springfield, Virginia 22151 – Price $3.00

RADAR CROSS SECTION AND OPTICAL RADIATION FROM THE TRAILBLAZER IIa 9° HALF-ANGLE BLUNT NOSE CONE DURING HYPERSONIC REENTRY

By Wayne L. Darnell
Langley Research Center

SUMMARY

Data reduced from two radar and three optical radiation measurements made on a nose-cone configuration during a reentry test are presented and discussed. Brief theoretical explanations of the reasons for radar enhancement and optical radiation during reentry are included. The body, a 9° half-angle cone with a 12.32-inch-diameter (0.313 m) spherical nose and 19.17-inch-diameter (0.487 m) base, was reentered by the Trailblazer IIa vehicle and provided test data from an altitude of about 219,500 feet (66903.6 m) to 71,000 feet (21640.8 m) and a velocity range of 19,700 fps (6004.6 m/sec) to 10,000 fps (3048.0 m/sec).

UHF and S-band radar provided the cross section and trajectory information of this report. The reentry altitude over which cross-section enhancement due to plasma interaction occurred was as follows: beginning, 188,000 feet (57302.4 m) and 145,000 feet (44196.0 m); peak, 144,000 feet (43891.2 m) and 117,000 feet (35661.6 m); and end, 74,000 feet (22555.2 m) and 82,000 feet (24993.6 m) for the UHF and S-band radar cross sections, respectively. The lower frequency UHF radar cross-section enhancement was of greater magnitude as well as longer and peaked earlier than the S-band; these results are reasonable, based on the plasma phenomena involved. S-band static cross-section preflight tests on the cone indicated slightly lower values than were experienced in flight. Aspect angles could not be obtained by comparison of the S-band flight data with S-band static cross-section aspect-angle data.

Optical radiations recorded on two panchromatic films at different sites and on one blue-sensitive film provided data for the three light curves presented in this report. The reentry altitudes over which the optical data were recorded are: Beginning, 219,500 feet (66903.6 m), 194,000 feet (59131.2 m), and 188,000 feet (57302.4 m); peak, 85,500 feet (26060.4 m), 95,500 feet (29108.4 m), and 102,000 feet (31089.6 m); and end, 71,000 feet (21640.8 m), 76,000 feet (23164.8 m), and 79,000 feet (24079.2 m) for the panchromatic film at the Coquina site, panchromatic film at the Wallops site, and the blue-sensitive film at the Coquina site, respectively. The data from the two panchromatic films compared well in magnitude during most of the data interval but data from the blue-sensitive film were much fainter.

Comparison of the radar-cross-section and optical-magnitude curves showed that the radar enhancements occurred within the altitude interval of optical radiation and the enhancement peaks occurred earlier than the optical radiation peaks. The main fluctuations observed in the radar-cross-section and optical-magnitude curves were similar and may be accounted for by body motions as well as by plasma turbulence.

The radar-signal enhancements and optical radiations recorded for the reentry were reasonably substantiated by theory and compared well with other flights using similar body shapes and flight parameters.

INTRODUCTION

Since the man-made satellite and intercontinental ballistic missile (ICBM), much additional knowledge on the reentry of high-speed bodies into the atmosphere has been needed. Ground-test facilities were incapable of providing all the conditions necessary to simulate atmospheric reentry. It was necessary to devise a means of performing controlled experiments under actual reentry conditions. A series of such experiments have been conducted under the Trailblazer program.

The Trailblazer program was initiated to study the relation of velocity, material, and shape of a payload to its behavior during hypersonic reentries. This program consists of launching a series of rocket vehicles carrying small payloads of varying materials and shapes which reenter at different velocities. This project is a joint project of the National Aeronautics and Space Administration and of the Lincoln Laboratory of Massachusetts Institute of Technology in which the reentry data are obtained by special ground-based radars and optical instruments. The primary purpose of the radars is to measure the apparent target cross section as effected by the ionized gases surrounding the payload during its reentry. Simultaneously, the optical equipment records radiated light from the reentry. Radar and optical instrumentation also provided the payload trajectory.

One series of vehicles, designated Trailblazer I, has been launched and a complete description of nine of these vehicles is found in reference 1. A second series (Trailblazer II) is currently being launched. These vehicles are capable of accelerating a 40-pound (18.144 kilogram) payload to a velocity of about 20,000 ft/sec (6096.0 m/sec) at reentry. The payloads are partially instrumented and are built to survive to sufficiently low altitudes to conduct complete reentry studies. The first of this series, Trailblazer IIa, carried a 9° half-angle blunted cone payload coated with an ablative material. The objectives of the flight of this vehicle were to check the performance of the new series, to monitor the vehicle and payload motions by telemetry, and most important to reenter a payload to provide radar-cross-section and optical-radiation measurements and subsequent reentry analysis.

It is known that during these high-speed reentries, the radar-cross-section measurement indicates values far in excess of that for the bare target. This

phenomenon of signal enhancement has been attributed to the ionized reflecting gases which form around the payload and stream behind it. These same gases are thought to be the most significant source of optical radiation so that one is led to expect some similarities between the radar and light data. Such similarities could be helpful in establishing better time connections between radar and light data occurrence and, in general, adding to reentry information.

In this report the reentry radar-cross-section and optical-radiation data from the 9° half-angle blunted cone are presented. This presentation is preceded by some theoretical discussion which is included to provide a better understanding of the meaning of these reentry data. The cross-section and radiation data are then discussed and compared to discover the similarities, if any, that exist between them.

It is not intended that absolute measurements between the optical energy and radar energy received be compared. Emphasis is placed on the comparison of the location and relative magnitude of the various peaks of the rationalized curves of the optical-radiation and radar-cross-section data.

SYMBOLS

Measurements for this investigation were taken in the U.S. Customary System of Units. Equivalent values are indicated herein in the International System (SI) in the interest of promoting use of this system in future NASA reports. Details concerning the use of SI, together with physical constants and conversion factors, are given in reference 2.

A aspect angle (measured between body axis and radar line of sight), degrees

A_a approximated aspect angle (approximated value for early reentry only), degrees

A_{VV} velocity-vector aspect angle (measured between velocity vector and radar line of sight), degrees

C_D drag coefficient

C_p specific heat at constant pressure, Btu/lb-$^{\circ}$F (joules/kg-C$^{\circ}$)

e electron charge, 1.602×10^{-19} coulomb

f_p plasma frequency (characteristic frequency), cps $\left(8.970\ (N)^{1/2}\right)$

I_X moment of inertia about X-axis (roll-axis), slug-foot^2 (kg-m^2)

I_Y moment of inertia about Y-axis (perpendicular to roll-axis), slug-ft^2 (kg-m^2)

k	Boltzmann's constant, 1.38×10^{-23}, joule/molecule-^{o}K
K	radar constant, watts-ft^4-m^{-2} (watts-n. $mi.^4$-m^{-2})
k_a	index of absorption for air
k_p	index of absorption for plasma
M	Mach number
m	electron mass, 9.109×10^{-31} kg
n	number density of molecules, atoms, ions, number/$meter^3$
N	number density of electrons, electron/$meter^3$
P_r	power received at radar antenna, watts
R	reflection coefficient for power, normal incidence of electromagnetic wave on a homogeneous plasma slab
R_r	radar slant range, feet (n. mi.)
S	cross-sectional area of vehicle, sq ft (m^2)
S_e	collision cross-sectional area of molecules, atoms, and ions for electrons, $meter^2$
T	temperature, ^{o}K
W	weight, lb (kg)
x	distance along body axis measured from nose, in.(meters)
X,Y	coordinate axes
ϵ_o	electric permittivity of free space, 8.854×10^{-12} farad/meter
ϵ_r	electric permittivity relative to free-space value
η_a	index of refraction for air
η_p	index of refraction for plasma
ν	collision frequency of electrons with molecules, atoms, and ions, number of collisions/sec
ρ	weight density, lbm/ft^3 (kilograms/m^3)
σ_{ac}	ac electrical conductivity, mhos/meter

σ	radar-cross-sectional area, square meters
σ_{dB}	radar-cross-sectional area, dB relative to 1 square meter
ω_r	angular frequency of radar signal, radians/sec
ω_p	angular plasma frequency (characteristic frequency), radians/sec

THEORY

When a body enters the earth's atmosphere at hypersonic speeds its energy is greatly dissipated as thermal energy in the surrounding air molecules. This energy increases the internal energies of the air molecules and produces dissociation and atomic ionization. The result is formation of an ionized gas which can radiate light and interact with radar signals beamed at it.

Radar Data

Initially, the reentry body may be expected to provide an essentially specular return of the radar signals it intercepts (ref. 3). As heating and air ionization increase, the radar signal encounters an increasingly dense plasma shield around and trailing the body. During the most intense portion of the ionization, the radar-cross-sectional measurement may become dependent upon the electromagnetic reflection characteristics of the plasma and relatively independent of the bare-body cross section.

A detailed treatment of the interaction of electromagnetic waves with plasmas providing the absorption, reflection, and transmission conditions is beyond the scope of this report. This information, however, is available; for example, see references 4 and 5.

With simplified conditions, the plasma characteristics which provide signal reflection can be easily visualized. Consider the free electrons in the plasma to be oscillators free to move about equilibrium positions established by their electrostatic fields. In a homogeneous plasma a natural frequency of oscillation exists for these free electrons. The frequency ω_p is called the plasma frequency (ref. 6) and is defined as

$$\omega_p^2 = \frac{e^2 N}{m\epsilon_o} = \left(2\pi f_p\right)^2$$

where e is the electron charge, N is the number density of the electrons, m is the electron mass, and ϵ_o is the electric permittivity of free space. Since e^2, m, and ϵ_o are constants, ω_p is directly proportional to the square root of N. A damping factor is present which affects the freedom of the electron oscillations. This damping is the result of the frequent

collisions which an electron makes with surrounding molecules and atoms. The collision frequency ν can be stated (from ref. 7) as

$$\nu = \left(\frac{8kT}{m}\right)^{1/2} \sum n_i S_{e,i}$$

The number density n of molecules, atoms, and ions of each specie i with which the electron can collide must be summed as well as the velocity-averaged collision cross section S_e which each species presents to the moving electron to determine the collision frequency of the electron. Temperature T is in ^{o}K and k is Boltzmann's constant.

When the plasma frequency compared with the radar signal frequency as in initial reentry is low, the radar power reflected from the plasma is very small or insignificant. This condition corresponds to the weakly ionized plasma (underdense) and is little changed from ambient air. At the point in a reentry where the plasma frequency has risen to approximately that of the radar signal (critical point), the reflective ability of the plasma may increase greatly. A further increase of the plasma frequency can cause the plasma to become highly reflective (overdense) if the collision frequency (damping) does not become too large relative to the plasma frequency.

Consider an idealized case of a plasma slab uniformly ionized and of semi-infinite extent. A plane-polarized radar wave normally incident on such plasma has a reflection coefficient R given as follows:

$$R = \frac{\left(\eta_a - \eta_p\right)^2 + \left(k_a - k_p\right)^2}{\left(\eta_a + \eta_p\right)^2 + \left(k_a + k_p\right)^2}$$

where

$$\eta_p^2 = \frac{1}{2}\left[\epsilon_r + \sqrt{\epsilon_r^2 + \left(\frac{\sigma_{ac}}{\omega_r \epsilon_o}\right)^2}\right]$$

$$k_p^2 = \frac{1}{2}\left[-\epsilon_r + \sqrt{\epsilon_r^2 + \left(\frac{\sigma_{ac}}{\omega_r \epsilon_o}\right)^2}\right]$$

$$\sigma_{ac} = \frac{Ne^2}{m} \frac{\nu}{\omega_r^2 + \nu^2}$$

$$\epsilon_r = 1 - \frac{\sigma_{ac}}{\nu \epsilon_o}$$

The index of refraction of air η_a is taken as 1 whereas the coefficient of absorption of air k_a is taken as zero. (The index of refraction is defined as the square root of the dielectric constant.) Applying these equations to the UHF and S-band radar frequencies given in table I yields the curves shown in figures 1 and 2. In figure 1, reflection coefficient R is plotted as a function of plasma frequency, collision frequency being used as a parameter for a UHF radar frequency. In figure 2 a similar set of curves are plotted for an S-band radar frequency. It may be noted that as the collision frequency increases, the reflectivity decreases for a constant value of plasma frequency. Furthermore, the plasma frequency required for reflection of the UHF radar is lower than that required for reflection of the S-band radar. This idealized conception of plasma effect has been oversimplified in many ways. Some of the simplifications are

(1) The boundary of the plasma is not a sharp interface of the optical type

(2) The plasma is not a homogeneous media but may vary in electron density, chemistry, and thickness throughout

(3) The incident radar waves are not necessarily normal to the shock wave or plasma; thus, reflection coefficients and "optical" refractions are difficult to assess

(4) Incident radar waves may undergo phase and polarization changes at plasma boundaries.

Optical Data

Visible radiations during reentry are generally emitted from three areas: the gas cap (ref. 8), the reentry body surface (ref. 9), and the wake (refs. 7 and 10). Gas-cap radiation intensity is related to body velocity, ambient density, and body size and shape. Except for high altitudes, this radiation is generally considered to be very small in comparison with the wake radiation. Body surface radiations are dependent on the spectral emissivity and temperature distribution on the body. The intensity of these radiations can be relatively significant at high altitudes before wake radiations are well established but generally become dominated by the wake later.

The character of radiation emitted in the wake varies with the rate at which recombinations of the dissociated and ionized materials can occur and the types of materials available for recombination. These materials are provided by the gas cap and body surface. At high altitudes (300,000 feet) (91440.0 m) the recombination rates are thought to be so slow as to be essentially frozen because of the low number densities of ions and electrons.

It has been shown in recent studies that the flow field behind a blunt body will not generally attain chemical equilibrium above an altitude of about 50,000 feet (15240.0 m) (refs. 7 and 10). Based on such information, the reentry period considered herein would be expected to display the radiation characteristics of nonequilibrium. For the case of a nonequilibrium wake,

little recombination generally occurs in the pressure expansion behind the reentering body, and thus a cool type of wake is produced. Several seconds may be required for the recombinations at 200,000 feet (60960.0 m) producing a long wake. This wake will be relatively insensitive to temperatures and wake enthalpy but could be very affected by ablation materials.

For the reentry at altitudes of 200,000 feet (60960.0 m), radiations would be expected to occur from the gas cap, the body surface, and from far back in the wake. At lower altitudes (150,000 feet) (45720.0 m), the forward wake will become more radiative as the number densities of ions and electrons increase and thus produce a faster recombination time. As the conditions of the equilibrium wake are approached, the wake becomes hotter and more radiative close to the body. Radiation intensity becomes more temperature sensitive and turbulent mixing in the wake may occur and may result in optical scintillations.

VEHICLE AND REENTRY BODY DESCRIPTION

Vehicle

The Trailblazer II vehicle is essentially a four-stage solid-fuel rocket system with the motors arranged in tandem. The third and fourth stages are mounted in a structural shell (velocity package) and face in a rearward direction at launch. The complete vehicle is shown in figure 3(a), and a cut-away view of the velocity package, in figure 3(b). During second-stage firing, the canted fins of the rocket spin the remaining system to maintain the attitude of the velocity package at approximately 65° (up from the launch horizontal) throughout the remainder of the flight. After second-stage firing, the velocity package separates and coasts to apogee.

When the velocity package has passed apogee, the third stage fires and propels the third and fourth stages downward out of the open end of the structural shell. On the Trailblazer IIa (after third-stage burnout) a 15-inch (0.381 m) spherical rocket motor mounted in the rear of the payload was fired and accelerated the fourth stage (payload) to approximately 19,400 ft/sec (5913.1 m/sec). The trajectory of the Trailblazer has been designed to bring the reentry of the payload back toward the launch site to facilitate radar measurements. Additional information on the Trailblazer IIa vehicle can be obtained from reference 11 which covers the performance of several Trailblazer II vehicles during flight.

Reentry Body

The reentry body, a 9° half-angle blunted cone, is shown in figure 4. It consisted of three main components: an ablative shield and substructure, instrumentation, and an integral 15-inch (0.381 m) spherical rocket motor. The heat shield and substructure are shown in figure 5 in a cross-section view taken across the axis of the cone. The physical properties of the reentry body are listed in table I.

The heat-shield substructure was mainly HK 31A-H24 magnesium thorium alloy 0.050 inch (0.0013 m) thick with aluminum alloy (6061-T6) used for the nose. The hemispherical nose was covered with a molded phenolic nylon cap which varied from 0.300 inch (0.0076 m) thick at the nose center to 0.075 inch (0.0019 m) thick at the edges where the ablative layer on the skirt began. The skirt was coated with a transparent epoxy polysulfide 0.075 inch (0.0019 m) thick over the entire surface.

The ablation heat shield for the 9° cone was designed under contract to NASA and MIT-LL and a comprehensive analysis of the anticipated reentry behavior of the outfitted payload was carried out by the manufacturer. The heat shield was designed to protect the metal substructure of the reentry body down to the altitude of 80,000 feet (24384.0 m) for the most severe conditions, but the heat shield was not expected to burn through before an altitude of 70,000 feet (21336.0 m) to 60,000 feet (18288.0 m) for a nominal trajectory. The nominal velocity-altitude curve was obtained from the heat-shield manufacturer and is shown in figure 6 for comparison with the actual flight data given later. Preflight analysis of the heat-shield design indicated that if failure occurred, it would be due to complete ablation of epoxy polysulfide in the area just behind the phenolic-nylon cap. The thermal properties of both heat-shield materials are given in table I. Reentry heat-flux curves taken from the heat-shield analysis are presented in figure 6. These three curves are based on preflight predictions using the nominal flight trajectory and heat-transfer equations and tables of Lees, Eckert, Walker, and Brunner. Each of these curves indicates the body heat flux anticipated at the particular body location noted on the curve. The curve labeled $x = 6.24$ is representative of a position on the skirt of the cone located 6.24 inches back from the nose, measured along the body axis. This position is approximately where failure of the ablative coating was expected if it had occurred. The aerodynamic stability of the reentry body was expected to be good until an altitude of about 50,000 feet (15240.0 m) was reached; if thermodynamic failure did not occur, tumbling was expected below this altitude.

There were two types of instrumentation in the reentry body; a seven-channel frequency-modulated—phase-modulated telemeter and a light telemetry system composed of 6 flashing xenon lights.

DATA ACQUISITION EQUIPMENT

The flight tracking equipment which provided the reentry data consisted of a UHF (420 Mc) radar, an S-band (2800 Mc) radar, and three K-24 aerial cameras.

Radar

The S-band radar is a modified FPS-6 model specially built to skin track the small payloads of the Trailblazer I series and refined continuously since its initial installation. It can track a payload automatically and has the dual capability of position-coordinate measurements and return-signal-strength

monitoring. The UHF which is similar to the S-band was built to monitor the weak echo signal from small Trailblazer payloads but it has no tracking capabilities. It remains slaved to the S-band but is considered to be a valuable complement to reentry coverage because its low radar frequency is especially sensitive to plasma. The operating characteristics of each radar as measured for the 9° half-angle-cone flight are given in table II and a photograph showing the physical plant is shown in figure 7. The radars are located about 2.2 n. mi. inland from the launch site at the NASA launch facility at Wallops Island, Virginia.

Optical

Three K-24 cameras were used to produce the photographs. One of these cameras was modified to accept photographic plates instead of film and another was equipped with a controlled high-speed rotating shutter arrangement. This device provides an intermittent or chopped photographic image of the optical reentry which is accurately time spaced so that real-time and velocity calculations can be made. All the K-24 cameras were still types and used an f/2.5 lens setting. Their field of view was 38° and exposed a film area of about 5 inches by 5 inches (0.0013 m by 0.0013 m). A typical K-24 camera is shown in figure 8.

The photographs were chosen from among many on the basis of their quality and spectral coverage. Two types of films (spectral ranges) are used. Panchromatic film was loaded in two of the cameras and a blue-sensitive emulsion was used in the other. Spectral sensitivity curves of the two types are shown in figure 9. Both curves are based on only the wavelengths of light which would be passed through the camera optics. These curves both show a cutoff point at about 3600 angstroms. This point is the point where transmission ceases for the camera lenses.

The camera equipped with the photographic plate contained the blue-sensitive emulsion and was located at a NASA camera site at Coquina Beach, North Carolina. The shutter chopping camera also located at Coquina Beach, North Carolina, contained panchromatic film. The third camera located at the Wallops Island (Spandar) camera site used panchromatic film.

FLIGHT DATA

Trailblazer IIa was launched from the NASA Wallops Station in a southeasterly direction over the Atlantic Ocean during a period of maximum darkness on December 14, 1961. Its payload was fired downward from the burned out third stage at 379.2 seconds after lift-off and at an altitude of about 515,000 feet (156972.0 m). Near the end of burning of the previous stage (third-stage motor), some despinning and off-axis thrusting was shown by the third-stage telemetry. These conditions produced a wobbling of about 7.7° as reported in reference 11. The exact amount of wobble transferred to the payload could not be determined by the xenon light system or telemetry of the payload as planned. The strength of the payload telemeter signal decreased to the noise level and the lights

were not visible. It is thought that the disk-shaped telemetry antenna-light reflector mounted on the motor nozzle was damaged when the payload exited out of the third-stage adapter because of the wobble.

Radar Data

Radar trajectory data were reduced from the S-band target position readings, made to the nearest 0.0055° in angle and 0.00382 nautical miles in range, at 40 times per second. Poor quality position data at some points during the reentry required considerable smoothing by the computer before suitable results were produced. A spherical earth system was used and corrections were made for oblateness.

Flight data from the S-band radar are presented in figures 10 to 14. Figure 10 is a Lambert conformal conic projection of the flight area off the eastern coast and shows the launch site, the radar locations, and all camera sites. The dashed line is a surface projection of the entire trajectory. The projection of the trajectory in a vertical plane along the flight azimuth is given in figure 11. The portion of reentry trajectory which is most pertinent to this report is plotted in figure 12. The variation of velocity with altitude from just before the fourth-stage firing through reentry is also on the plot and for comparison the optical velocity data are included. Finally, the altitude intervals where radar enhancement and optical radiation are thought to have occurred are indicated to provide a comparison with the important trajectory variables. Radar antenna tracking angles and altitude variation with flight time for the incoming payload are given in figure 13.

The angle relation between the radar antenna axial line extended to the target and the velocity vector of the target is designated the velocity-vector aspect angle A_{VV} and is represented graphically in sketch (a).

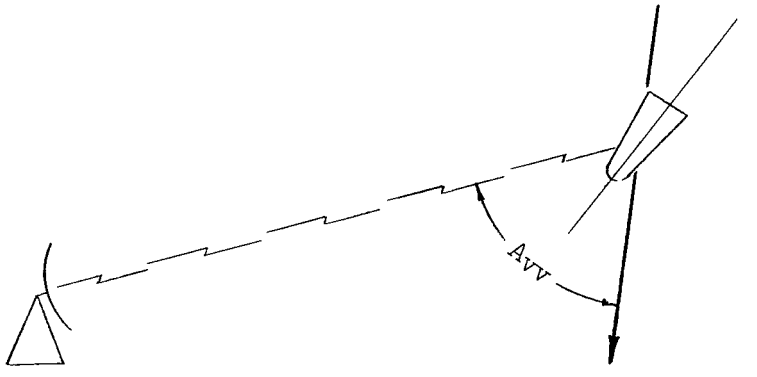

Sketch (a)

The variation of the velocity-vector aspect angle with reentry altitude of the payload is shown in figure 14. This angle should not be confused with the actual aspect angle A of the payload which is defined as the angle between the radar antenna axial line and the longitudinal axis of the body as shown in sketch (b).

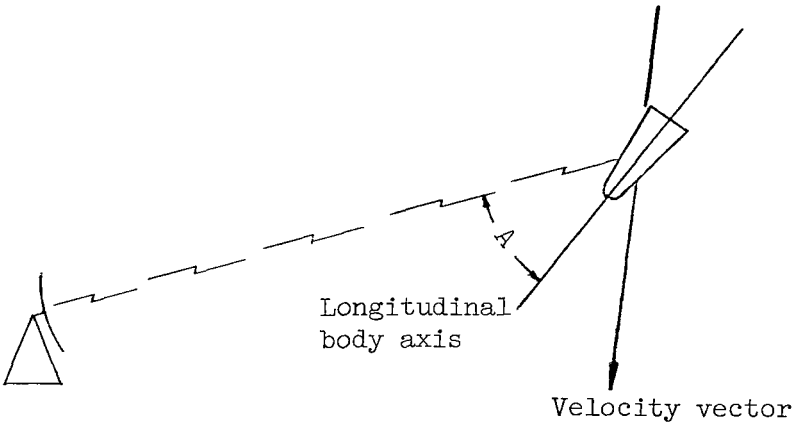

Sketch (b)

These two angles become equivalent when the aerodynamic forces on the reentry body aline its longitudinal axis with the velocity vector.

Measurement of the flight-path angle at velocity-package separation shows that the vehicle attitude was spin stabilized at 65.7° above the launch horizontal. If this vehicle attitude was maintained properly, the aspect angle of the reentry body during early descent could be approximated by the value of 65.7° minus the value of the elevation angle of the radar antenna at the time. This approximated aspect angle A_a is plotted for comparison with the velocity-vector aspect angle A_{VV} in figure 14.

Optical Data

Flight data were reduced from measurements on the photographic image of the reentry streak. By using the positions of the known stars found along the light trail, the optical-site coordinates, and the camera pointing angles, the reentry streak is positioned in space. (See ref. 12.) The velocity of the reentering body is deduced from the photographs containing a shutter-chopped image. Optical trajectory reductions from different plates on one flight commonly agree to within a few percent. The optical velocity reduction is presented in figure 12.

DATA REDUCTION METHODS

Radar Cross Section

Radar intermediate-frequency-amplifier voltages from the UHF and S-band radars are monitored throughout the flight each time a signal pulse is transmitted (320/sec). The peak value of each echo pulse from the logarithmic intermediate-frequency amplifier is digitized and recorded on magnetic tape for subsequent reduction to apparent target cross section in dB relative to 1 square meter.

Before the flight, the radar are calibrated to determine the relationship between the logarithmic intermediate-frequency-amplifier voltage pulses and the apparent radar-target cross section. Signals of known power are injected into the radar receiver and the corresponding logarithmic voltages of the intermediate-frequency amplifier are recorded and plotted to establish an S-shaped signal power-voltage curve for each radar. The signal power reflected from a standard target at given slant ranges is determined for each radar by tracking a 6-inch-diameter (0.0015 m) aluminum sphere carried aloft by a balloon. This information provides all the variables necessary to calculate the value of the radar constant K from the simplified standard radar equation

$$\sigma = \frac{P_r R_r^4}{K}$$

where σ is the target cross-sectional area in square meters, P_r is the received power in watts, and R_r is the slant range of the target from the radar in feet (meters). Further information on such calibrations can be found in reference 13.

The radar equation must be applied to each of the 320 readings per second to develop continuous values of apparent target cross section throughout the flight period. The target cross section σ is further reduced to decibels of cross-sectional area relative to 1 square meter by the equation

$$\sigma_{dB} = 10 \log \frac{\sigma(\text{square meters})}{1(\text{square meter})}$$

By using a method of weighted averaging, the cross-sectional data at 320 points per second is smoothed by reducing it to data at 10 points per second. The accuracy of the reduced data is dependent upon the accuracy with which the calibration operations were carried out, the scatter about the S-shaped curve for the variation of voltage with power, and especially the variation of final power with range which determines the value for K. The errors in these factors may amount to variations of several decibels relative to 1 square meter of cross section.

Some cross-sectional measurement error is known to result from the recording of signal-pulse heights instead of the area or signal energy

represented by the pulse. This error cannot be ascertained but is known to exist since pulse shapes fluctuate erratically.

Static Radar Data

Radar reflectivity measurements were made on the reentry body under simplified static conditions. The 9° half-angle cone configuration was mounted on a pedestal and rotated in position while being irradiated by radar at several frequencies; however, only the S-band frequency is discussed. The cone was located 20 feet (6.1 m) from a low-power continuous wave radar on an outdoor range to minimize background response. The cone was mounted at roll angles of 0° and 90° and was rotated through a full range of aspect angles. The body position for each of the roll planes is illustrated in figure 15. Both a horizontal and vertical plane of signal polarization were used.

Results from this test are presented in figure 16 where the aspect angle A varies from -12° to 122° and where 0° is the nose-on aspect angle. The planes of polarization are indicated on each figure as well as the roll angle of the cone. Cross-sectional measurement accuracy was estimated to be ±1 dB.

The oscillations prevalent in these curves are mainly cyclic. A complete cycle occurs for an angle change of 3° to 10° and may result in a cross-sectional change of up to 16 dB. These curves indicate the sensitivity of the radar cross section to the orientation of the body with respect to the radar. The angle cross-sectional relations differ slightly from one polarization to another and from one initial body position to another 90° from it. The maximum cross-sectional area of 6 dB occurs at an aspect angle of nearly 81° on all the curves, and is the broadside view of the 9° half-angle cone; the minimum cross-sectional area varies from curve to curve and the angle which produces it is different for each curve. The actual geometric cross section of the nose cone at an aspect angle of 90° is approximately $0.26m^2$ (-5.8 dB) and the minimal geometric cross section (end view) is $0.19m^2$ (-7.2 dB). It is clear then that the curved surface of the nose cone and the sharp edges around the antenna can cause significant attenuations or enhancements of the radar signal as it is moved through various aspect angles. Any angular motions of this cone in reentry prior to plasma effects would be expected to produce analogous results on its radar cross section.

Optical Radiation Magnitude

Relative optical magnitude radiated from the reentry body at any point along its trajectory was determined by viewing the photographic image with a densitometer. This instrument provides comparative readings of light transmittance through the photographic image of the reentry streak to that through the photographic images of surrounding stars. Since the visual magnitudes of these stars are available from star catalogs, a visual stellar magnitude-light transmittance curve can be established. This curve provides a relative magnitude value for each of the light transmission (densitometer) readings made on

the photographic image of the reentry streak. The relative magnitudes of each of the points on the trail are then corrected for velocity and atmospheric absorption. The relative magnitudes of the reentry streak are adjusted to values they would have if observed at a standard distance of 100 kilometers. Detailed methods of reduction are given in references 12 and 14.

Optical-magnitude reduction errors begin with the transmission readings. The gross fog of the emulsion determines the minimum level of fluctuation for which transmission readings can be applied. Below this level, small variations in these readings must be regarded as being due to the gross fog or granularity of the emulsion. A second consideration of data accuracy involves the curve fitting of the S-shaped-transmission—stellar-magnitude calibration. The scattering of data near the curved portions may allow calibration errors of 0.5 to 0.75 magnitude although the straight-line portion of the curve provides high accuracy; thus, those reentry-streak transmission readings which fell above or below the straight-line portion of the calibration curve may contain an error of up to 0.75 magnitude if the star readings were necessarily scattered. The third area of possible error is in the determination of the magnitude corrections for elevation angle, range, and velocity; these errors would depend on the range of values over which these corrections must be made. Notable among these corrections is the elevation-angle correction for which the errors are greatest for the smallest angles of elevation. Localized low-lying mists or fogs may make otherwise good elevation-angle correction data erroneous.

RESULTS AND DISCUSSION

Radar Data

Target cross-sectional variation with reentry altitude is seen in figures 17 and 18. These figures have been plotted from data at 10 points per second. The maximum fluctuation due to errors in recording and reducing the data at 320 points per second is thought to be ±2 dB. Because averaging tends to smooth the data, errors in the data at 10 points per second are probably less than ±1 dB. Fluctuations exceeding this amount are especially predominant in the S-band data but are nearly lacking in the UHF cross-sectional data.

Fluctuations greater than ±1 dB are believed to be caused mainly by two actions: the variation of the aspect angle of the nose cone A and the influence of the plasma during the radar-enhancement interval. During the free fall of the body prior to reentry but following burnout of the payload rocket motor, the bare-body cross section was being measured without plasma interference. During this period the curves for the S-band static cross section (fig. 18) should be useful in predicting the cross section to be expected. For this time interval of about 16 seconds (384 seconds to 400 seconds), the reentry body fell from 455,000 feet (138684.0 m) to 145,000 feet (44196.0 m) and caused the approximated aspect angle A_a (as suggested by the curve of fig. 14) to vary from about 40° to 57°. It will now be assumed for purposes of a brief analysis that the wobble of the reentry body about its wobble axis did not exceed $\pm 10^\circ$. This flight condition can be compared with the static data for the case of the

S-band radar by inspecting figure 16 between angles of about 40° and 57° and by considering variations of 10° to be attributed to wobble. Cross-section fluctuations between -9 dB and -17 dB are shown by the static curves and average values appear to decrease gradually from about -12 dB to -14 dB. This result compares poorly with the S-band flight data between 455,000 feet (138684.0 m) and 145,000 feet (44196.0 m) and is about 5 dB above the static dB level in general. This disagreement may be accounted for as follows: the actual value of the aspect angle A was greater than the approximated value A_a because the attitude angle of the vehicle increased during thrusting; the random motions of the wobbling body cannot be expected to fall continuously into the limited orientations of roll and polarization presented in figure 16. In addition, it is suggested that the wider disagreement of the static and flight data for altitudes from 225,000 feet (68580.0 m) to 144,500 feet (44043.6 m) is due to an increase of the aspect angle A of the body due to the aerodynamic forces. The actual aspect-angle value was probably in the region between the two curves of figure 14.

Aerodynamic forces became effective on the nose cone before 215,000 feet (65 532 m) as shown by the decrease in the velocity curve of figure 12. These forces would have dampened the wobble action of the payload and eventually alined its roll axis with the flight path. These aerodynamic effects are investigated (by computer programing) in reference 15. By using calculated preflight parameters and the body characteristics of the Trailblazer IIa payload, an envelope of total yaw angle beginning at a reentry altitude of 240,000 feet (73152.0 m) was calculated. Based on the input conditions used, wobble and angle of attack were found to become insignificant at an altitude between 80,000 feet (24384.0 m) and 90,000 feet (27432.0 m); thus, the body-aspect-angle value of 81° would be expected to occur below an altitude of 80,000 feet (24384.0 m). At this aspect angle, the maximum bare-body cross-section value shown on the static curves would occur. Before this occurrence, however, the influence of the plasma phenomena became the dominant factor and masked the variations of cross section of the bare body due to aspect-angle change.

Radar enhancements are evident on both of the radar cross-section curves but the UHF curve shows an enhancement which is of larger magnitude, longer, and occurs at a higher altitude interval than the S-band enhancement. The UHF enhancement period is judged to begin at about 188,000 feet (57302.4 m), peak at 158,000 feet (48158.4 m) and 144,000 feet (43891.2 m), and end about 74,000 feet (22555.2 m) altitude. This period covers an altitude interval of 114,000 feet (34747.2 m); therefore, the peak values occur approximately one-third of the way through the altitude interval of enhancement. The S-band cross-section enhancement is judged to begin at an altitude of about 145,000 feet (13716.0 m), peak at altitudes of about 125,000 feet (38100.0 m) and 117,000 feet (35661.6 m), and end at an altitude of about 82,000 feet (24993.6 m). This enhancement period covers an altitude interval of 63,000 feet (19202.4 m) and peaks more than one-third of the way through the altitude interval of its enhancement.

The presence of the many medium-sized fluctuations in the S-band radar cross section not found on the UHF curve is thought to be due to the higher frequency signal transmitted from the S-band radar. Greater definition of the wobbling target should be possible when viewed with 10.7-centimeter wavelengths (S-band) than with 71.4-centimeter wavelengths (UHF).

The large fluctuations in both radar curves are caused by the plasma sheath. The points where the value of ω_p approximates the value of ω_r of each particular radar are not readily evident but have been chosen as the points where the radar enhancements (listed previously) began and ended for each radar.

It has been seen that the UHF radar signal was more enhanced by the ionization phenomena than the S-band radar signal. This result is reasonable to expect on the basis of the theoretical plasma and radar-frequency relationship illustrated in figures 1 and 2. It was shown that the UHF radar signal is strongly reflected from a plasma slab for a value of ω_p approximately one-tenth of that required for the S-band.

The altitude of peak-signal enhancement for these radars appears to be fairly consistent with calculated and similar reentry flights at 20,000 feet per second (6096.0 m/sec) or less and with similar body design. Real-air hypersonic flow parameters based on velocity and altitude conditions have been calculated in a program by Huber. (See ref. 16.) Electron-density and plasma-frequency values are provided at the following three points in the flow field considered independent of the reentry body shape: normal shock flow (for equilibrium thermochemistry), far wake (for equilibrium thermochemistry), and the far wake (with frozen chemistry). When the flight values of velocity and altitude for the 9° cone were applied, the peak values of electron density and plasma frequency occurred near an altitude of 120,000 feet (36576.0 m) for all three flow-field points. Electron densities generated at these points reached from 10^{13} to 10^{14} electron/cm^3 ($\omega_p \approx 10^{10}$) at the normal-shock point (equilibrium chemistry). In reference 7 similar results are shown from flight tests made by the RAM B-3 vehicle which carried S-band microwave reflectometers in the nose of its 9° blunt-nose-cone payload.

The complementary effects of the shock-wave plasma and the wake plasma produce the cross-section enhancement. Two different radar frequencies are expected to have differing cross-section values from the same reentry. Because of the complexity of the reflection from and absorption in the actual plasma around and trailing the body, a sophisticated mathematical treatment is required for even approximate theoretical values for the net radar cross sections to be expected during a reentry. This treatment of the Trailblazer IIa payload is considered beyond the scope of this paper. The UHF radar cross-section value for the bare target before reentry is fairly well defined by the flight data as about 0 dB (1 square meter). This same value is approached again after the reentry is complete; thus, the nose cone may have remained intact.

Optical Data

The panchromatic photographic image of the reentry streak is shown in figure 19 enlarged about four times. This image is shutter chopped at the rate of 10 times per second. The visible reentry recorded by this film lasted approximately 8 seconds; however, the main shutter of the camera was open for 200 seconds to record the stars shown as short traces in the background. The camera was located at the Coquina site.

A second panchromatic photographic image of the reentry streak which is not chopped is presented in figure 20. This photograph was taken from the Wallops Island Spandar camera site and is enlarged approximately 8 times to obtain a comparable size. Total film exposure time was 100 seconds and the reentry trail lasted about 8 seconds.

Figure 21 shows the blue-sensitive photographic image of the reentry streak enlarged about 4 times. This image is noticeably fainter than that of figures 15 and 16 and is the result of its differing spectral sensitivity. It should be noted that the photographs of figures 19 and 21 came from the same type of camera located at essentially the same point (Coquina Beach camera station). The visible reentry recorded by this plate lasted only 7 seconds. The main shutter of this camera was open for 180 seconds and no shutter chopping occurred during the reentry portion although one long post-calibration chop can be seen on the star images.

The photographic magnitude data reduced from figures 19, 20, and 21 are presented in figures 22, 23, and 24, respectively. The magnitude curves of figures 22 and 23 are derived from the panchromatic films and that of figure 24 is the result obtained from the blue-sensitive emulsion on the photograpic plate. Calibration and correction errors on data in figures 23 and 24 probably do not exceed ±0.60 magnitude at the most and in general are much less. Errors in the magnitudes given in figure 22 reach ±1.0 magnitude at the lower altitudes because of elevation-angle corrections but most of the curve should be comparable with those of the other figures. Only the larger fluctuations in these curves are attributed to variations in the overall light intensity being radiated. The smaller fluctuations become questionable in their meaning. Two possibilities are suggested: (1) the variables of gross fog and reduction correction may produce such undulations; (2) the variations may be due to reentry body motions and to gross variations in the plasma radiations. The second possibility is felt to be the main cause but fluctuations due to the first possibility must not be overlooked. A wobbling reentry body will tend to form a precessing elliptical cylinder as a wake behind it. (See ref. 17.) This varying shape may well affect the light emission reaching the film and produce delayed variations related to body motions.

The light-emission period of the reentry, as demonstrated by these curves, begins at an altitude of about 194,000 feet (59131.2 m) and continues to an altitude of about 71,000 feet (21640.8 m) for the combined panchromatic films, but only for altitudes from 188,000 feet (57302.4 m) to 79,000 feet (24079.2 m) for the blue-sensitive emulsion. It should not be inferred that the total altitude interval of 123,000 feet (37490.4 m) represents the entire length of the optical streak recorded. Transmission readings on the photographic image are restricted to the interval where it is distinct enough for positive evaluation. Examination of the photographic image of figure 19 revealed that the streak was visible about 31,000 feet (9448.8 m) above the point where the data reduction began at 188,500 feet (57454.8 m). This result places the first sensing of light at an altitude of 219,500 feet (66903.6 m) and it is expected that light was emitted at an intensity below the threshold value of the film at a slightly higher altitude.

The peak of light radiation from the nose cone seems to cover an altitude range from slightly over 100,000 feet (30480.0 m) (blue-sensitive film) to

slightly over 80,000 feet (24384.0 m) (panchromatic film). The earlier peak of the blue-sensitive film could be explained by its pronounced blue sensitivity as opposed to the additional red to yellow light seen by the panchromatic film. More of the greater energy transitions (blue light) appear to be available before an altitude of 100,000 feet (30480.0 m) than after. The assumed cool wake radiations may be more effective blue light radiators than the hotter shorter wake which becomes prevalent toward the end of reentry. By this assumption the red wavelength radiations must be associated more with a wake which is closer to equilibrium conditions. Theoretical temperatures in the normal-shock area taken from Huber's curves (ref. 16) indicate a maximum at about 120,000 feet (36576.0 m) but it is known that nonequilibrium wake radiation is not especially temperature sensitive. The reentry body flux curves (fig. 6) indicated that the maximum body heating should occur at altitudes between about 100,000 feet (30480.0 m) and 90,000 feet (27432.0 m). This preflight calculation appears to correlate favorably with light intensity maximums received. The relationship between light intensity received and body heat flux would be assumed to be associated more closely at this lower altitude since it is closer to the equilibrium chemistry condition.

Comparison of Radar-Cross-Section and Optical-Magnitude Data

Comparisons of radar-cross-section and optical-magnitude data are based on the features of their reentry curves as follows: (1) the altitude interval of the reentry data, (2) the altitude at which the peak cross sections occurred compared with that at which peak light magnitudes occurred, and (3) the fluctuations in the data.

The altitude intervals over which both radar and optical reentry data occurred depend on the choice made for the beginning and ending of the reentry data. It has been judged that the first optical radiations registered began at an altitude of about 219,500 feet (66903.6 m) on panchromatic film and continued until an altitude of about 71,000 feet (21640.8 m) when they became too dim to register. This interval of altitude of 148,500 feet (45262.8 m) more than covers the interval of about 188,000 feet (57302.4 m) to 79,000 feet (24079.2 m) recorded by the blue-sensitive film. In comparison the combined radar altitude interval judged as reentry data extends only from about 188,000 feet (57302.4 m) to about 74,000 feet (22555.2 m) (or 114,000 feet (34747.2 m) total). The UHF radar is responsible for this coverage since the S-band radar extended only over altitudes from 145,000 feet (44196.0 m) to 82,000 feet (24993.6 m). These data are arranged graphically in figure 25. The band of energy wavelengths for which each of these receivers is sensitive is also shown. It is seen that the optical data not only covers a wider interval than the radar enhancement but it also covers the interval that includes all radar-enhancement data.

The altitudes at which the maximums occur on the radar curves and optical curves are indicated by diamond symbols on the respective lines in figure 25. It will be noted that the radar peaks occur more in the upper part of the reentry interval whereas the light data peaks occur in the latter part of the reentry interval.

The frequencies of the fluctuations of the optical and radar data have been studied; their variation is between 1.5 to 4 cycles per second. Radar curves show an increasing trend through reentry which begins around 2.5 cps for the UHF data and reaches 3.5 cps whereas that for the S-band data varies only from 1.75 cps to about 2.5 cps during reentry. This trend is not present in the optical data which begin at about 3 cps and rise rapidly to 3.5 cps for the panchromatic film and begin at 4 cps and drop to 3.5 cps for the blue-sensitive film. These fluctuation rates might be due to the wobble cycle. Because data oscillations are not better matched and the static cross-section tests show that oscillations can be produced merely by aspect-angle change without wobble, some reservation should be used.

CONCLUSIONS

A 45.31 pound (20.552 kilogram) ablative-coated cone with a 12.32-inch (0.313 m) spherical nose diameter and 19.17-inch-diameter (0.487 m) base was reentered at 19,700 feet per second (6004.6 m/sec) by a Trailblazer IIa rocket vehicle. Radar cross-section enhancements and optical radiations were recorded during this reentry test, some of which are reported and discussed herein. Optical radiations began at an altitude of 219,500 feet (66903.6 m) and continued to an altitude of 71,000 feet (21640.8 m) as recorded by panchromatic film. Blue-sensitive film recorded radiations at altitudes from 188,000 feet (57302.4 m) to 79,000 feet (24079.2 m). The UHF frequency radar enhancement was judged to have begun at an altitude of 188,800 feet (57302.4 m) and to continue to an altitude of 74,000 feet (22555.2 m) whereas S-band radar enhancement began at an altitude of 145,000 feet (44196.0 m) and extended to an altitude of 82,000 feet (24993.6 m).

Comparisons of these radar and optical data showed the following:

1. Radar enhancements occurred essentially within the altitude interval of the optical radiations.

2. The peak values of both radar enhancements presented occurred near the middle of the total reentry interval while the peak values of all the three optical data curves presented occurred at altitudes which were quite low in the reentry altitude interval.

3. Fluctuations in both radar and optical data were similar in frequency although they did not occur synchronously, and the fluctuations appeared to be due to the motion of the reentry body and to plasma turbulence.

4. These test results could be reasonably substantiated by theory and compared well with other flight-test data presented.

Langley Research Center,
National Aeronautics and Space Administration,
Langley Station, Hampton, Va., September 2, 1965.

REFERENCES

1. Gardner, William N.; Brown, Clarence A., Jr.; Henning, Allen B.; Hook, W. Ray; Lundstrom, Reginald R.; and Ramsey, Ira W., Jr.: Description of Vehicle System and Flight Tests of Nine Trailblazer I Reentry Physics Research Vehicles. NASA TN D-2189, 1964.

2. Mechtly, E. A.: The International System of Units - Physical Constants and Conversion Factors. NASA SP-7012, 1964.

3. Brinks, Walter J.: Relationship Between Specular Reflection Patterns and Reflecting Body Shape. TR-1040, Diamond Ordnance Fuze Lab., Dept. Army, Aug. 3, 1962.

4. Evans, John S.; and Huber, Paul W.: Calculated Radio Attenuation Due to Plasma Sheath on Hypersonic Blunt-Nosed Cone. NASA TN D-2043, 1963.

5. Swift, Calvin T.; and Evans, John S.: Generalized Treatment of Plane Electromagnetic Waves Passing Through an Isotropic Inhomogeneous Plasma Slab at Arbitrary Angles of Incidence. NASA TR R-172, 1963.

6. Goldberg, Philip A.: Electrical Properties of High-Altitude Ionized Shock Waves. Plasma Physics, James E. Drummond, [Compiler], McGraw-Hill Book Co., Inc., c.1961, pp. 245-269.

7. Huber, Paul W.; and Sims, Theo E.: The Entry-Communications Problem. Astronaut. Aeron., vol. 2, no. 10, Oct. 1964, pp. 30-38. (Available also as NASA RP-384.)

8. Öpik, Ernst J.: Physics of Meteor Flight in the Atmosphere. Interscience Publ., Inc. (New York), 1958.

9. Allen, H. J.; and Yoshikawa, K. K.: Luminosity From Large Meteoric Bodies. Smithsonian Contrib. Astrophys., vol. 7, 1961, pp. 181-193.

10. Hundley, R. O.: Air Radiation From Nonequilibrium Wakes of Blunt Hypersonic Reentry Vehicles. Memo RM-4071-ARPA (Contract NO. SD-79), The RAND Corp., June 1964.

11. Lundstrom, Reginald R.; Henning, Allen B.; and Hook, W. Ray: Description and Performance of Three Trailblazer II Reentry Research Vehicles. NASA TN D-1866, 1964.

12. Anon.: Papers on Reduction Methods for Photographic Meteors. Smithsonian Contrib. Astrophys., vol. 1, no. 2, 1957, pp. 183-243.

13. Kuhn, B. G.: Amplitude Calibration for Reentry Physics Program, Arbuckle Neck Radars. 21G-0015 (Contract AF 19(604)-7400), Lincoln Lab., M.I.T., Sept. 19, 1960.

14. Jacchia, Luigi G.: Photographic Meteor Phenomena and Theory. Tech. Rep. No. Three (Contracts NOrd 8555 and 10455), Harvard College Observatory and Center of Analysis, M.I.T., 1949.

15. Schippell, Herbert R.; Neal, Luther, Jr.; and Marcum, Don C., Jr.: Aerodynamic Characteristics of Two Trailblazer II Blunted 9° Cone Reentry Bodies at Mach 6.8 in Air and 21.2 in Helium. NASA TN D-2786, 1965.

16. Huber, Paul W.: Hypersonic Shock-Heated Flow Parameters for Velocities to 46,000 Feet Per Second and Altitudes to 323,000 Feet. NASA TR R-163, 1963.

17. Zeiburg, S. L.: Investigation of Phenomena Influencing Hypersonic Wake Analysis. DAMP Tech. Monograph No. 62-33, Missile and Surface Radar Div., Radio Corp. Am., Dec. 1962.

TABLE I.- PROPERTIES OF REENTRY BODY

Physical properties:	
Weight, lb (kg)	45.31 (20.56)
Location of center of gravity, inches (m) from nose along axis	12.52 (0.318)
I_Y, slug-ft^2 (kg-m^2)	1.15 (281.67)
I_X, slug-ft^2 (kg-m^2)	0.40 (34.08)
W/C_DA, lb/ft^2 (kg-m^2)	56.62 (659.59)
Minimum cross-sectional area (cone base), S, ft^2 (m^2)	2.005 (0.3735)
Drag coefficient (at M = 20), C_D	0.40
Thermal properties of phenolic nylon cap:	
Density, lb/ft^3 (kg/m^3)	75 (1201.38)
Effective heat of ablation, Btu/lb (J/kg)	4000 (9297777.6)
Ablating surface temperature, $^\circ$R ($^\circ$K)	1700 (1600.75)
Specific heat, Btu/lb-$^\circ$F (J/kg-$^\circ$C)	0.38 to 0.40 (1589.92 to 1673.60)
Thermal conductivity, Btu-ft/sec-ft^2-$^\circ$R (J/m-sec-$^\circ$K)	0.000032 (0.199246)
ρC_p, Btu/ft^3-$^\circ$R (J/m^3-$^\circ$C)	28.5 (1910098.09)
Thermal properties of epoxy polysulfide:	
Density, lb/ft^3 (kg/m^3)	79 (1265.46)
Ablating surface temperature, $^\circ$R ($^\circ$K)	960 (903.95)
Specific heat, Btu/lb-$^\circ$F (J/kg-$^\circ$C)	0.46 (1924.64)
Thermal conductivity, Btu-ft/sec-ft^2-$^\circ$R (J/m-sec-$^\circ$K)	0.00003 (0.18679)
ρC_p, Btu/ft^3-$^\circ$R (J/m^3-$^\circ$C)	35.5 (2435554.93)

TABLE II.- NOMINAL CHARACTERISTICS OF WALLOPS RADAR

	S-band	UHF
Wavelength, cm	10.7	71.4
Frequency, Mcs	2800	420
Antenna diameter, ft (m)	60 (18.288)	60 (18.288)
Gain, dB	52	35
Beam width, deg	0.38	2.9
Transmit polarization	Vertical	Vertical
Receive polarization	Vertical	Vertical/Horizontal
Tracking systems	Conical scanning	Slaved
Peak transmitter power, megawatts	4.0	8.0
Pulse length, μsec	2.2	6.0 and 1.0
Pulse repetition frequency, cps	320	320
Type receiver	Parametric	Parametric
Receiver band width, Mcs	0.6	1.8
Receiver noise figure, dB	3.5	1.6
Receiver minimum detectable signal, dB below milliwatt	-116	-120
Pointing accuracy, Mil (deg)	1 (0.056266)	----------
Range accuracy, yd (m)	±50 (±45.72)	----------

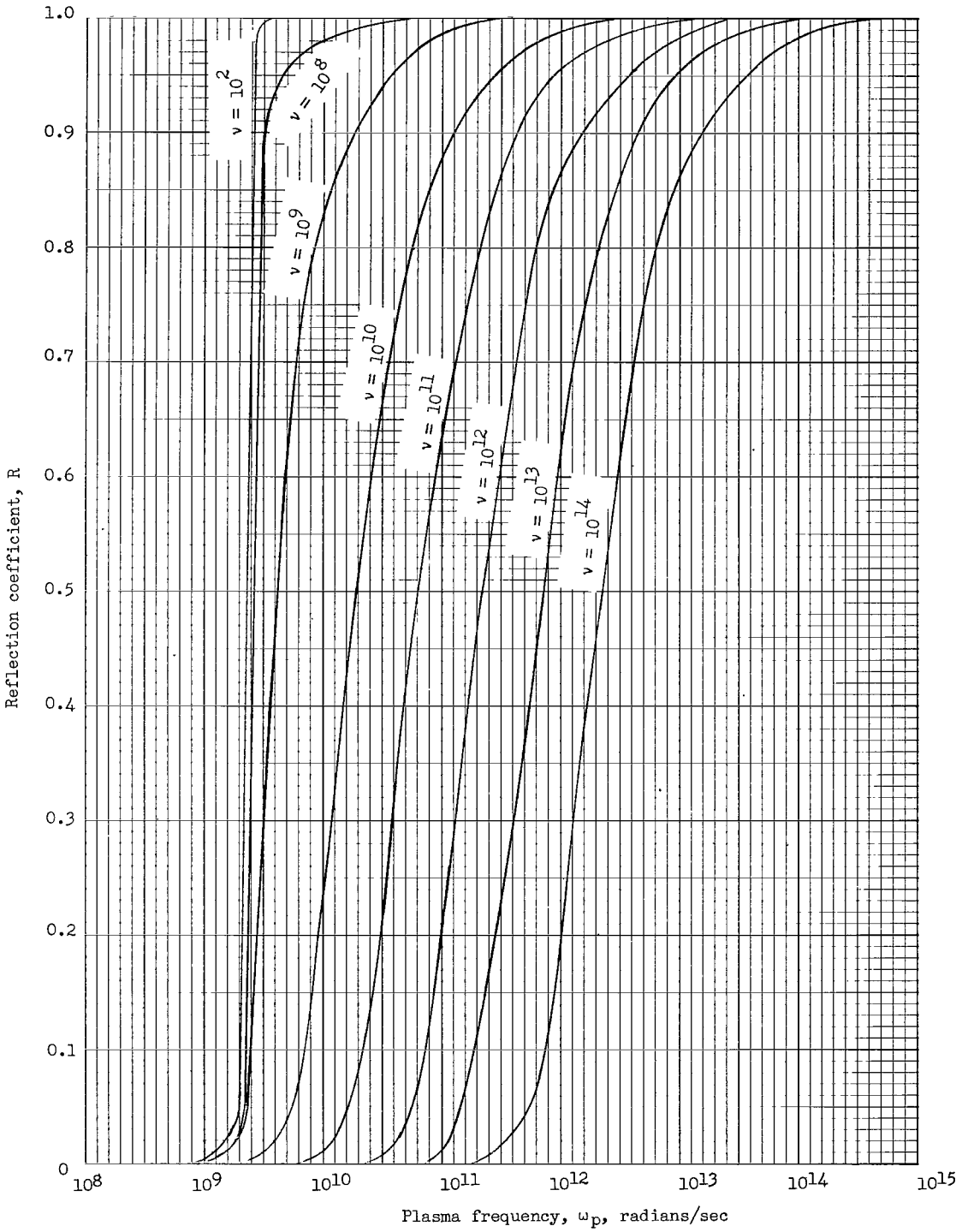

Figure 1.- Variation of reflection coefficient with plasma frequency for a theoretical thick plasma slab irradiated by UHF radar.

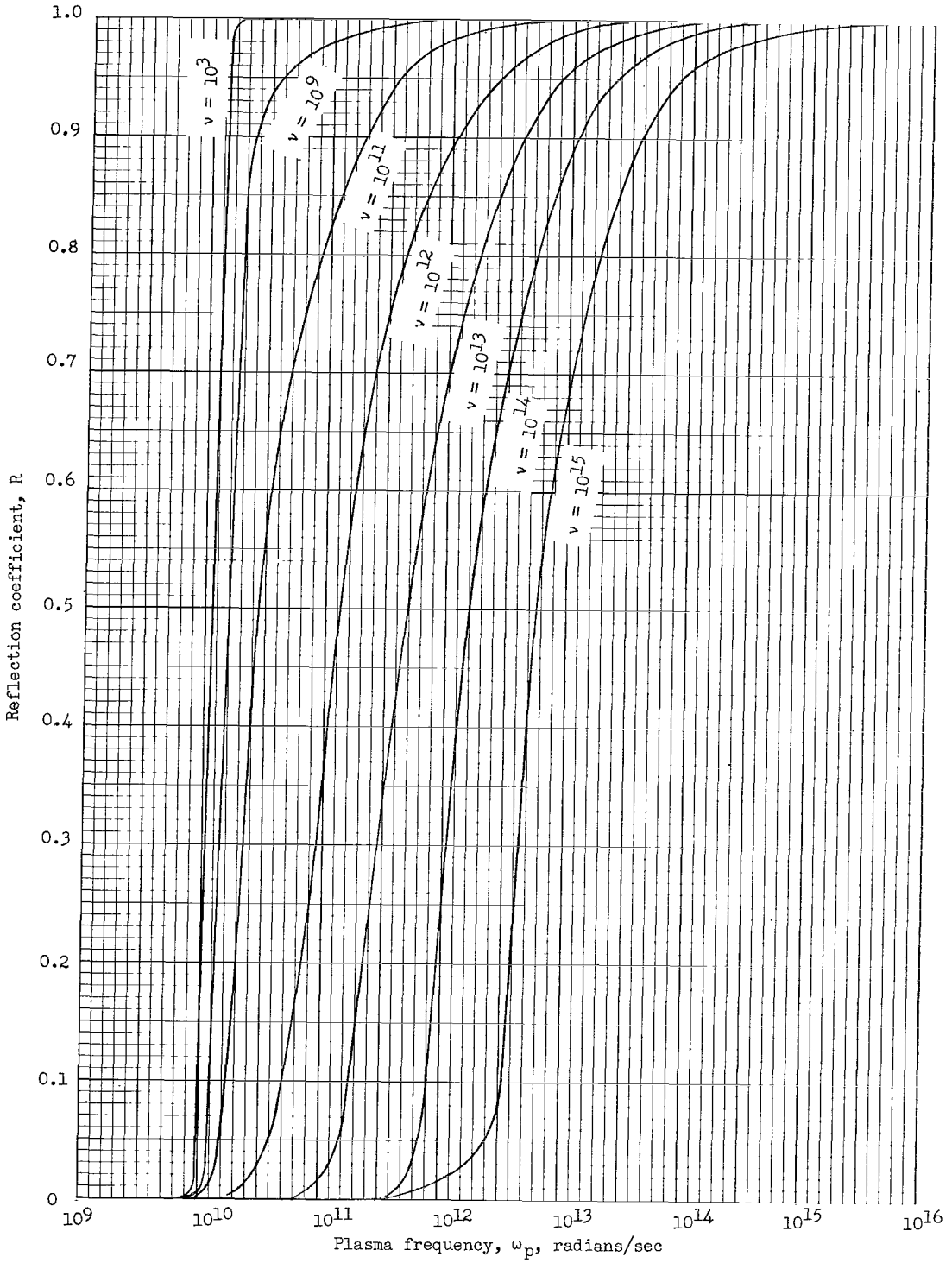

Figure 2.- Variation of reflection coefficient with plasma frequency for a theoretical thick plasma slab irradiated by S-band radar.

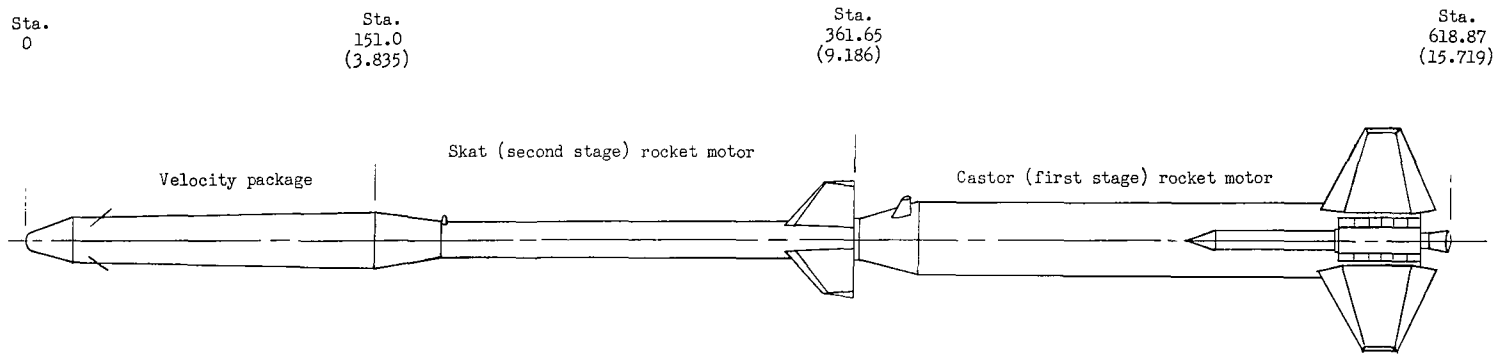

(a) First stage, second stage, and velocity package.

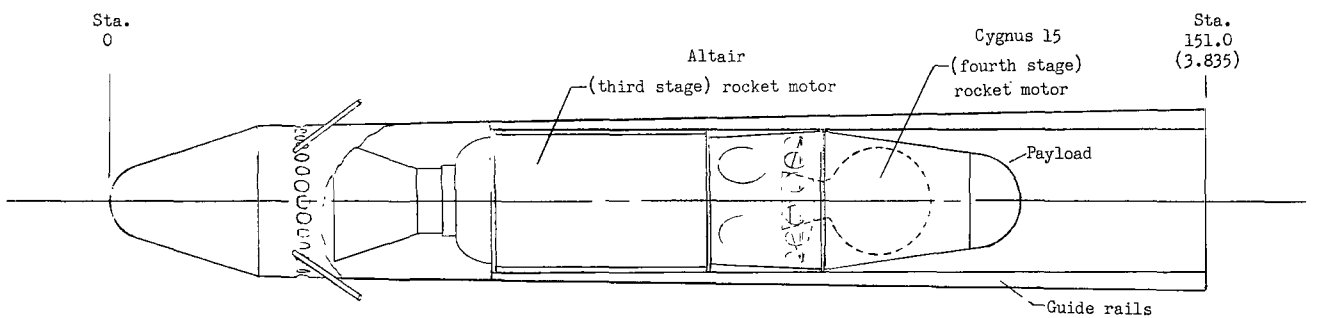

(b) Velocity package.

Figure 3.- Sketches of Trailblazer IIa vehicle. All station locations are in inches (meters).

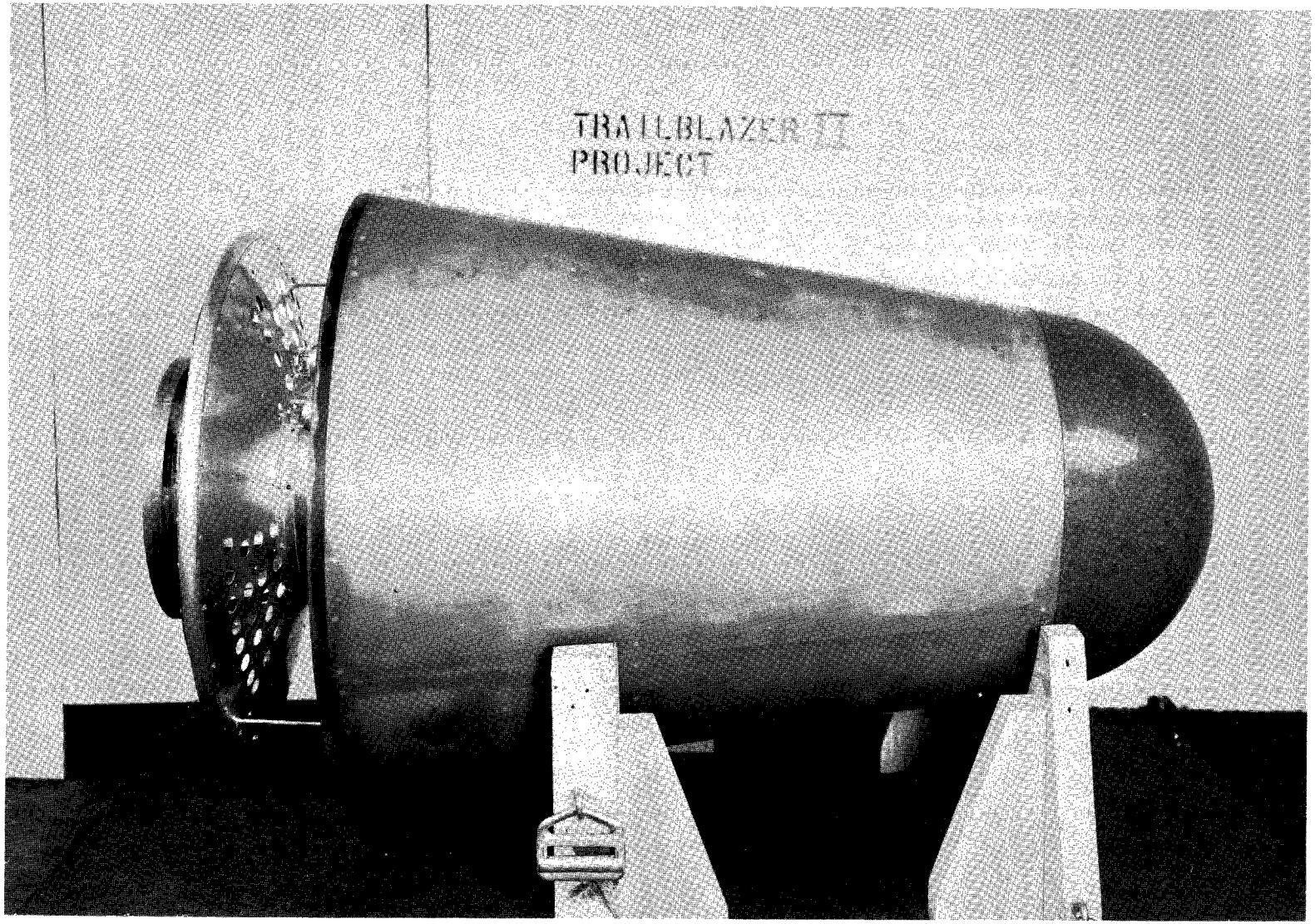

Figure 4.- Reentry body for Trailblazer IIa. L-61-7903

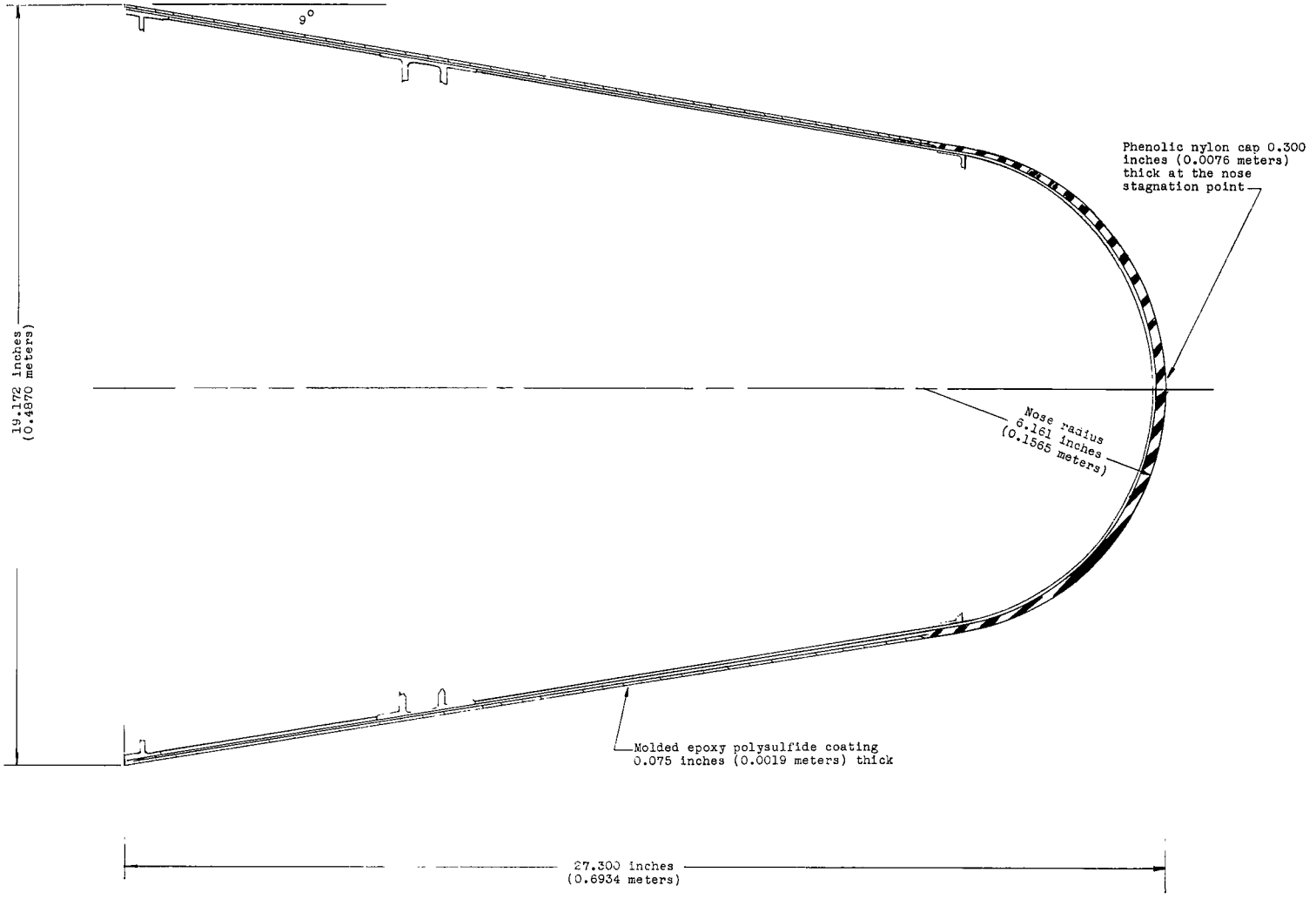

Figure 5.- Cross-section view of reentry body heat shield and substructure.

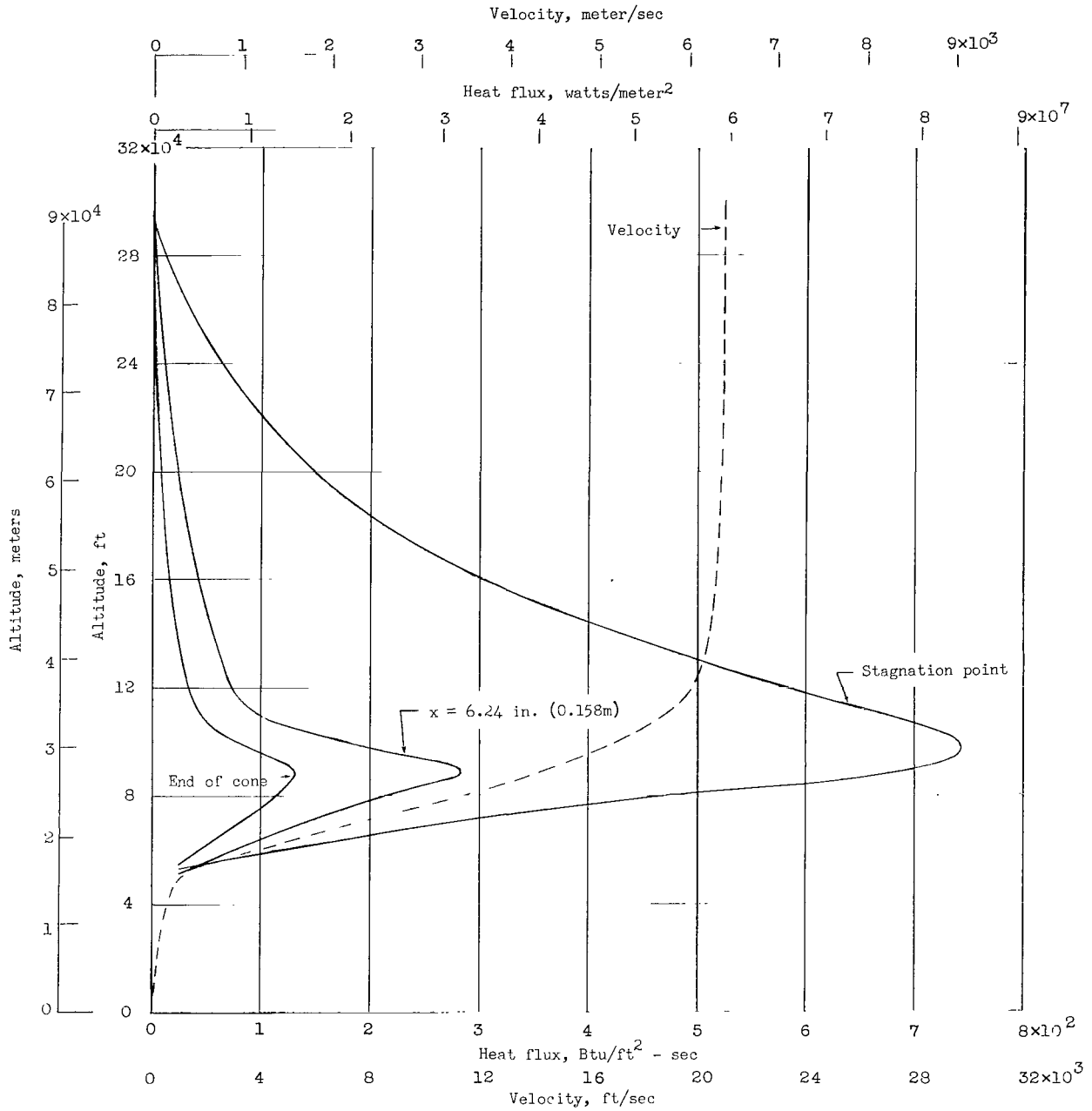

Figure 6.- Variation of heat flux with reentry altitude for 9° half-angle cone using nominal velocity-altitude curve shown for three positions on cone. (x is the axial distance measured from nose in inches (meters).)

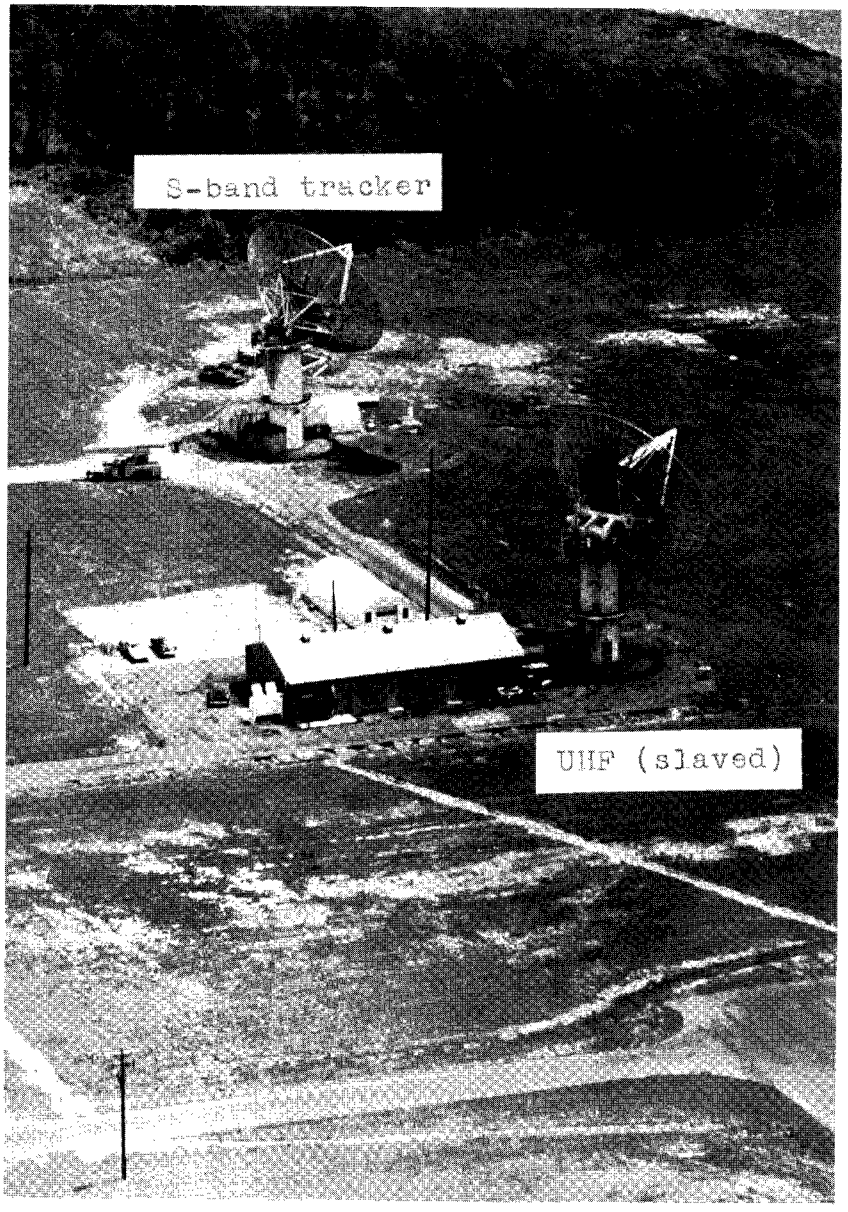

L-61-7209.1

Figure 7.- Radars located on mainland behind launch site on Wallops Island.

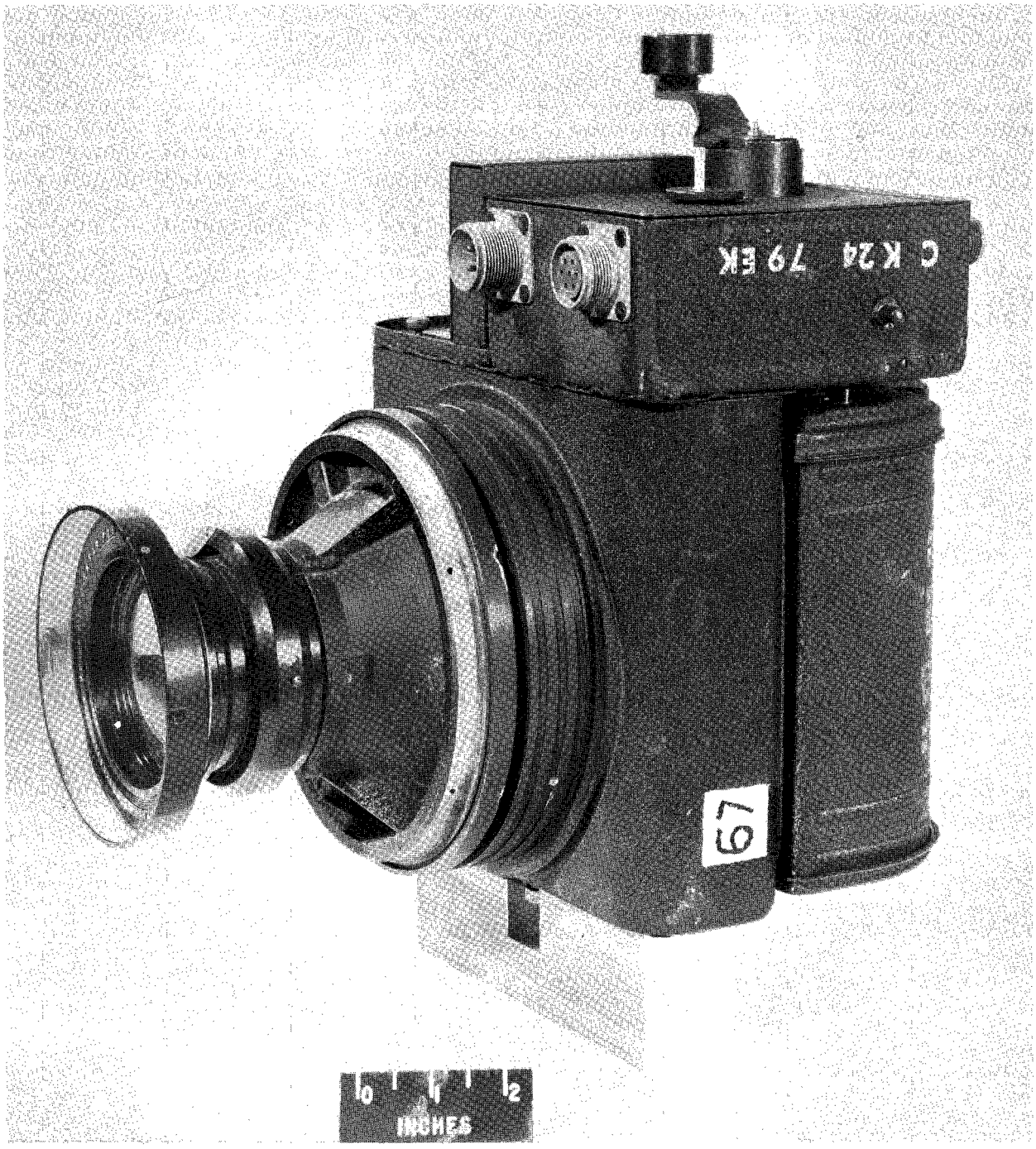

Figure 8.- K-24 aerial camera. No chopping shutter is used with this camera. L-65-1056

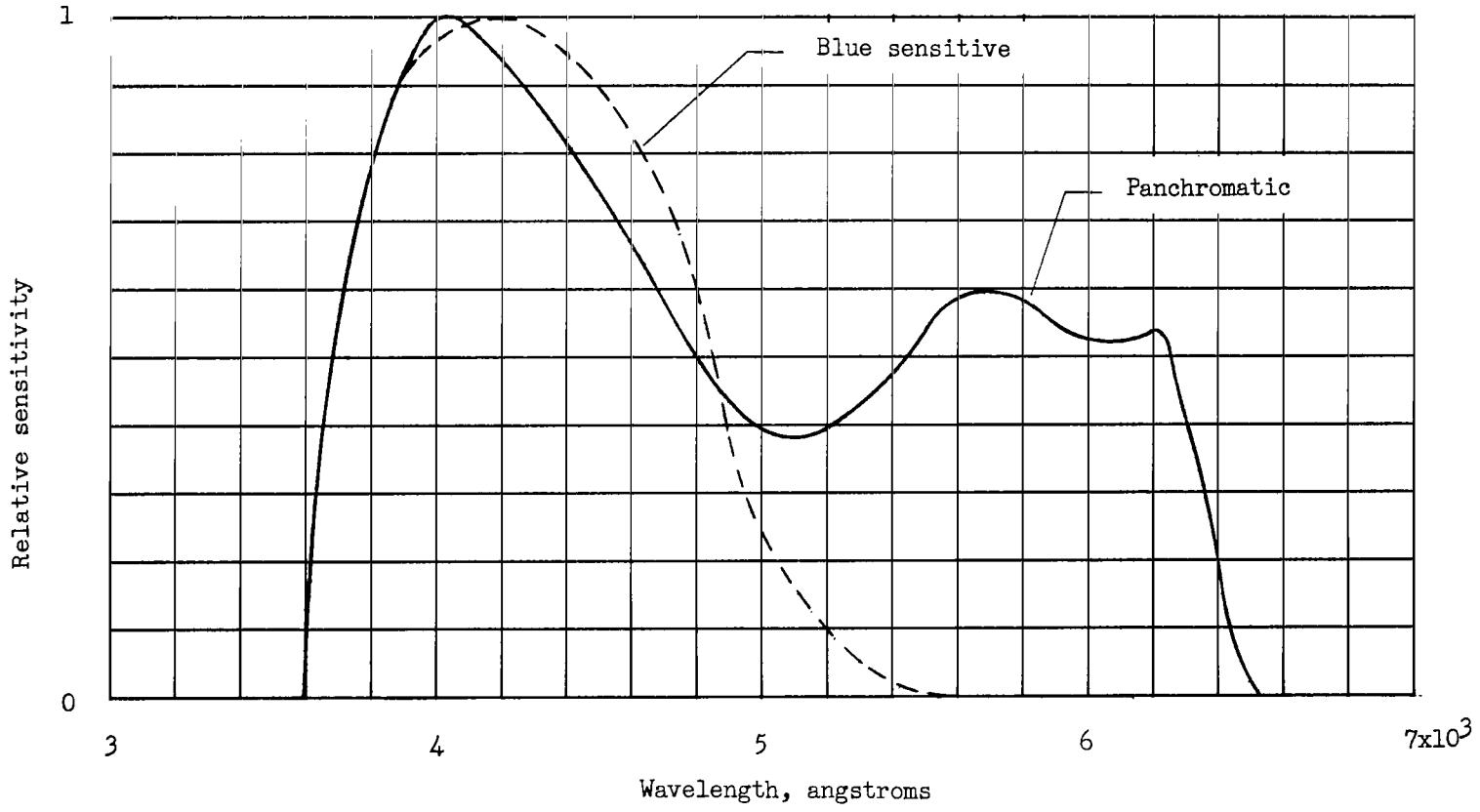

Figure 9.- Typical spectral sensitivities for panchromatic and blue-sensitive photographic emulsions to light passing through camera lens.

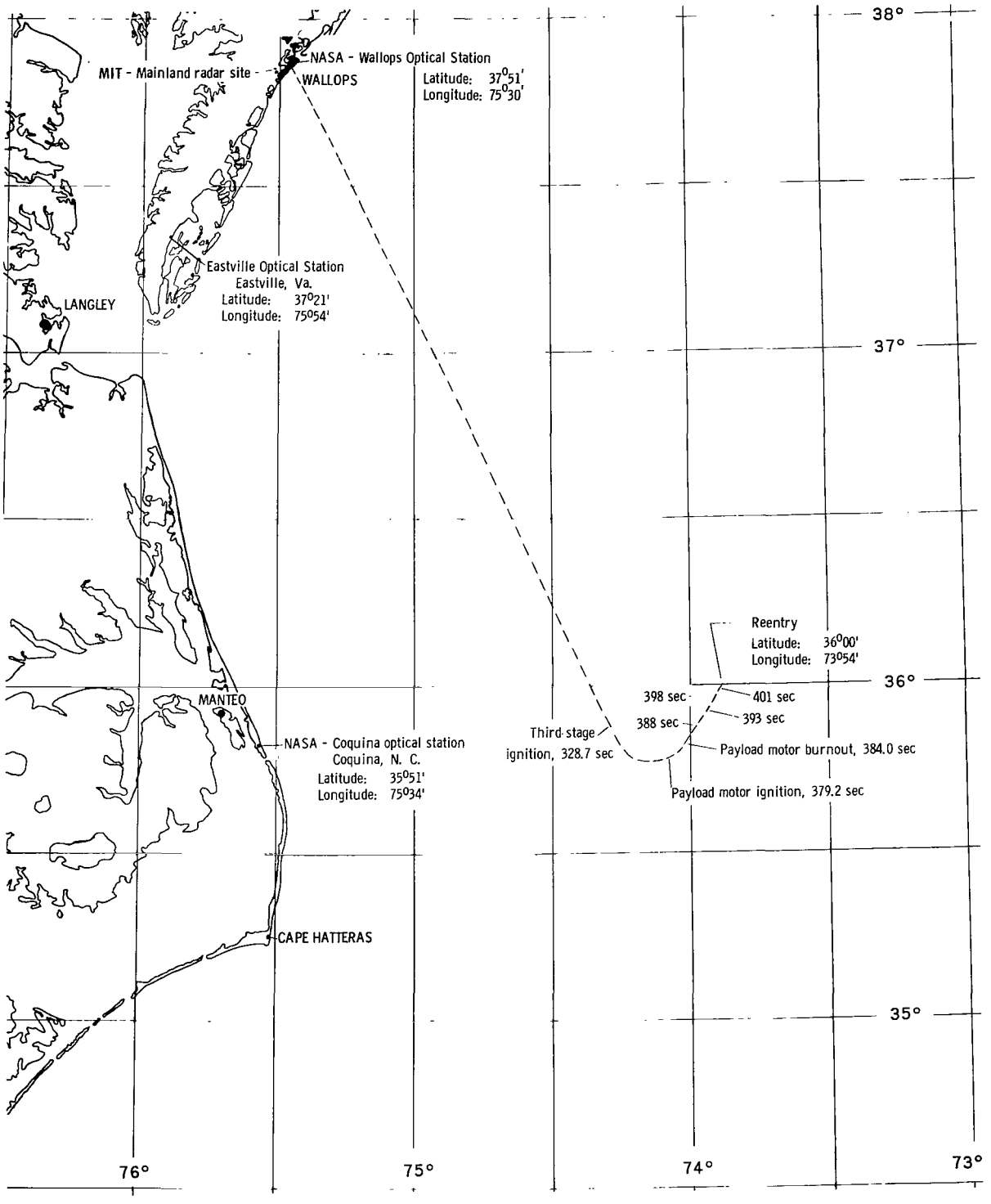

Figure 10.- Firing range for Trailblazer vehicle showing radar and optical tracking sites and surface projection of Trailblazer IIa flight trajectory.

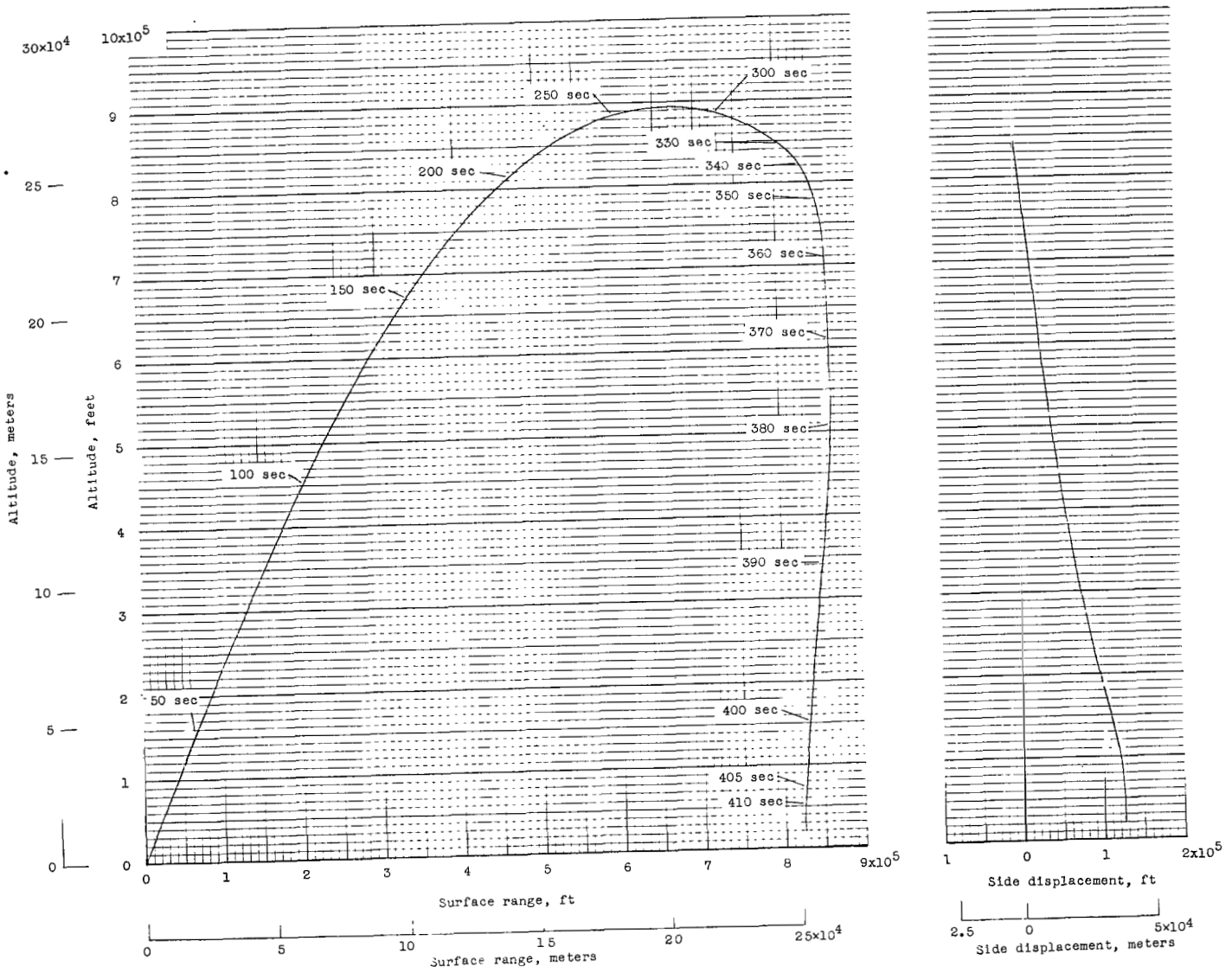

(a) Looking from side.

(b) Looking toward launcher.

Figure 11.- Vertical flight trajectory of reentry body.

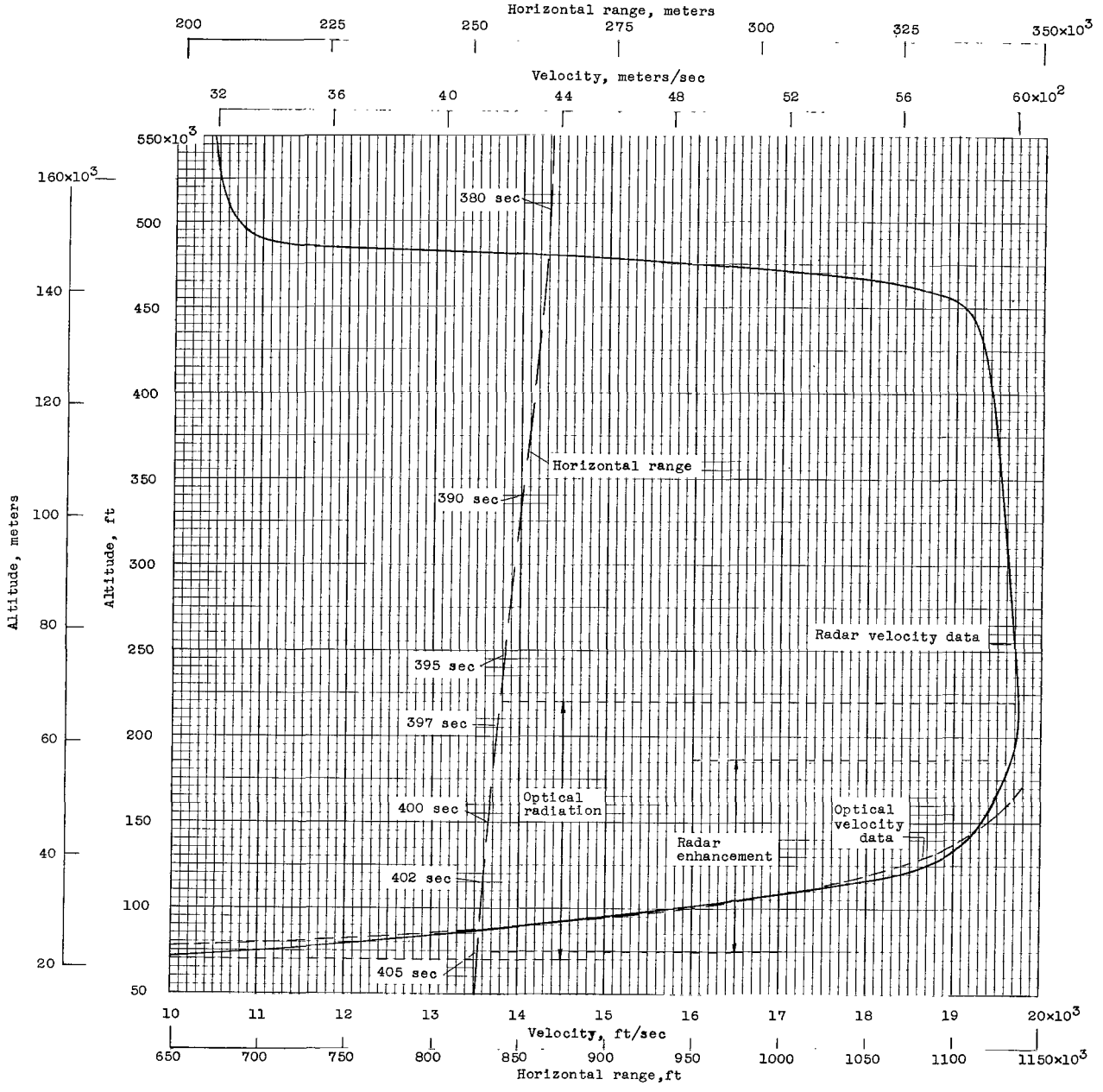

Figure 12.- Variation of velocity and horizontal range of reentry body with altitude from just before fourth-stage firing through reentry and showing period of radar enhancement and light radiation.

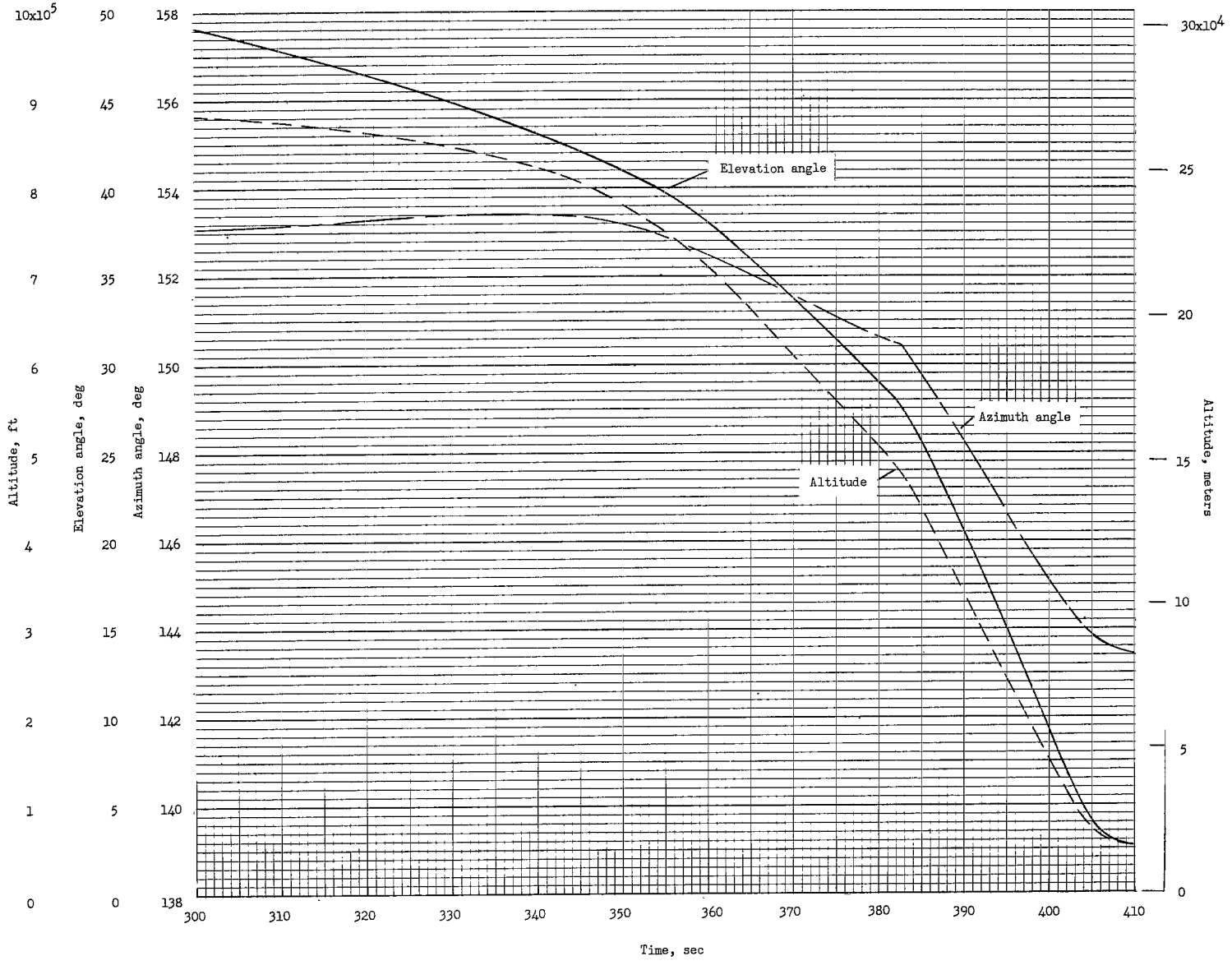

Figure 13.- Variation of radar tracking angles and altitude with flight time.

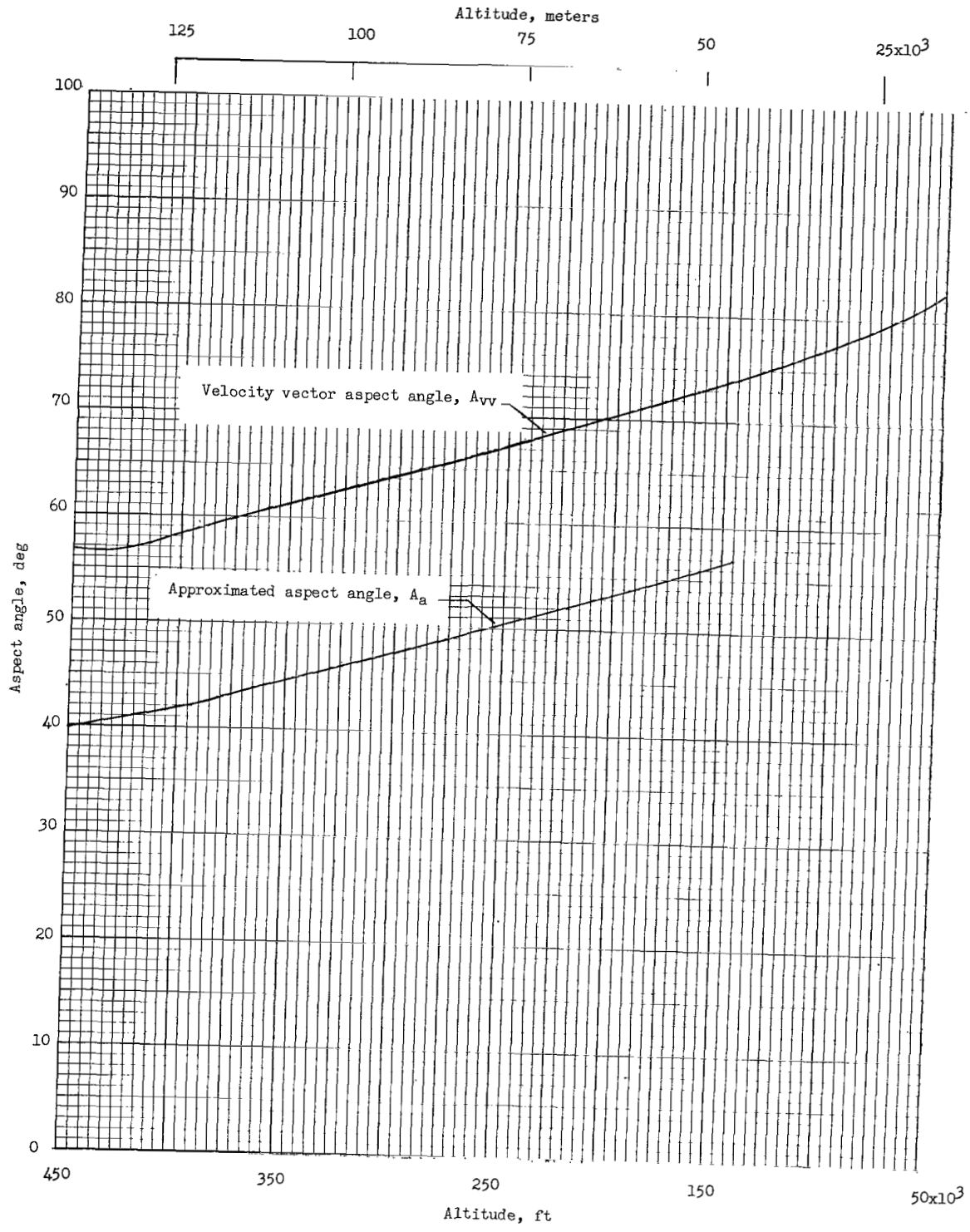

Figure 14.- Variation of aspect angle with altitude for reentry of 9° cone.

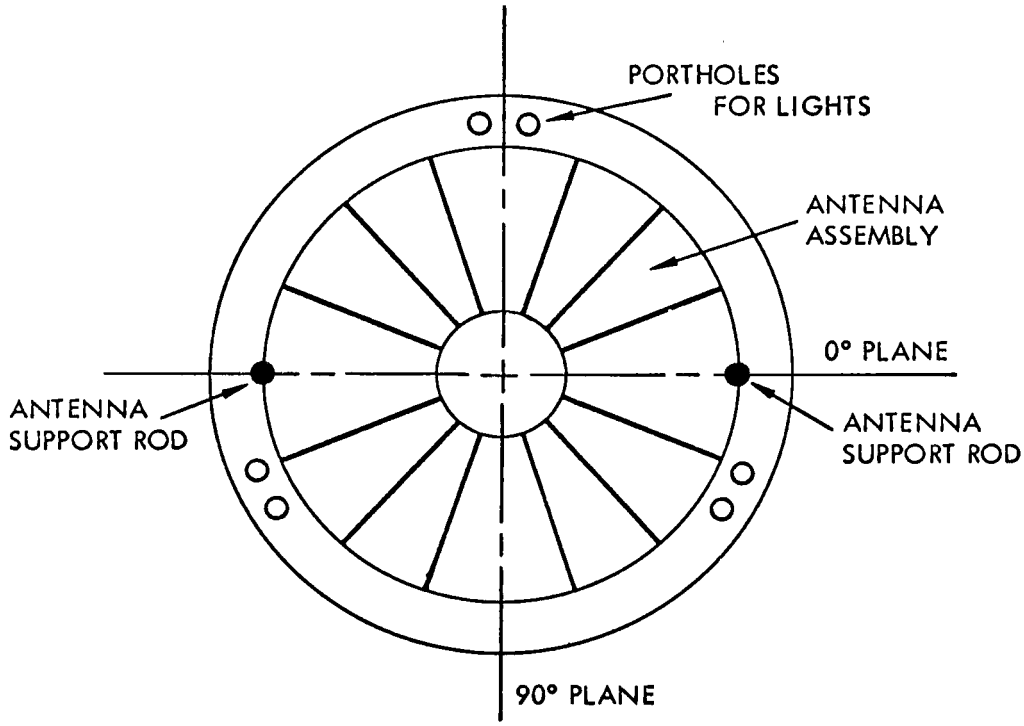

Figure 15.- Rear-view sketch of 9° cone reentry body showing roll planes for measurement of static cross section.

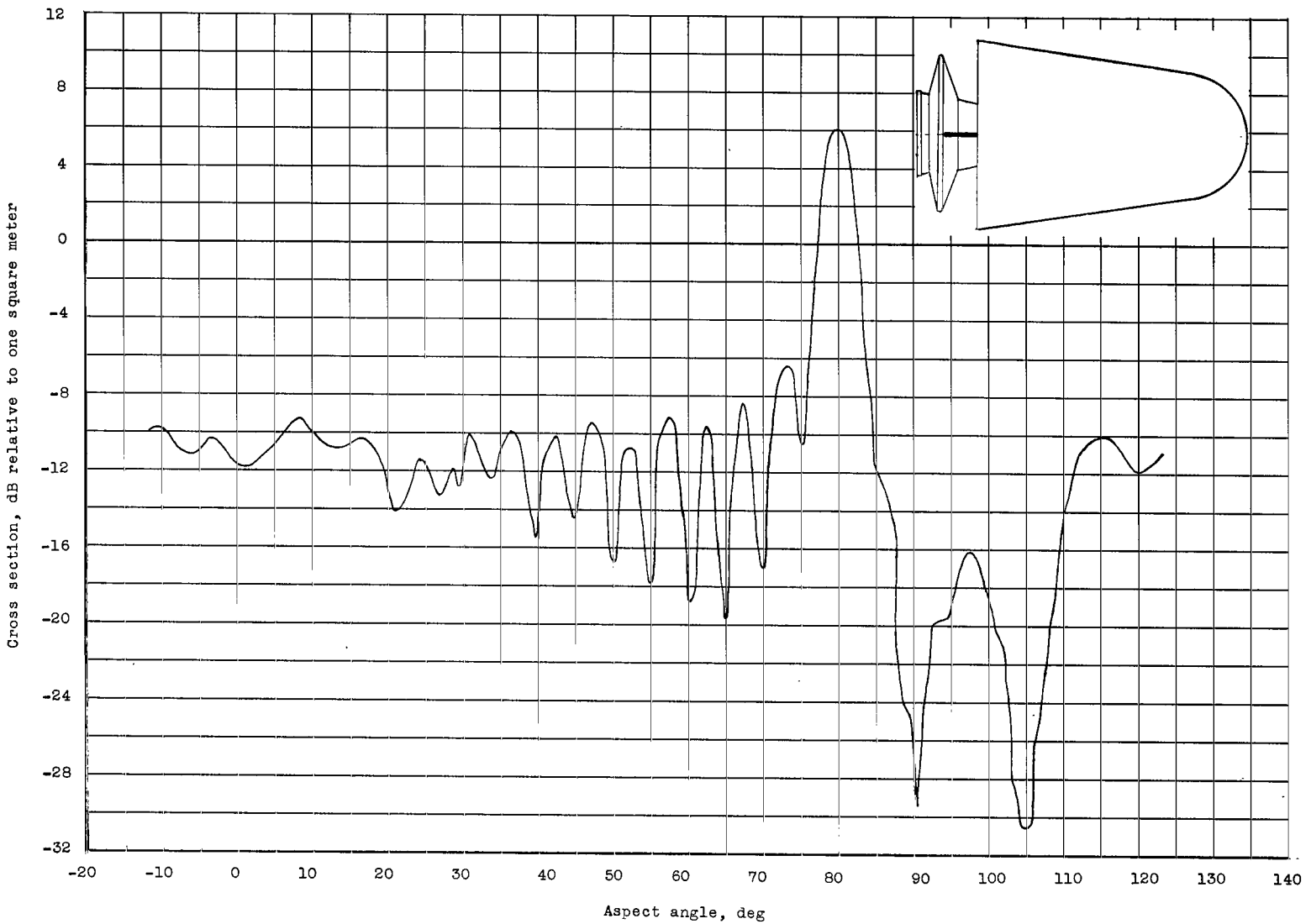

(a) Initial body position, roll 0° (antenna horizontal); radar polarization, horizontal-horizontal.

Figure 16.- S-band static radar cross-section variation with aspect angle for 9° half-angle cone.

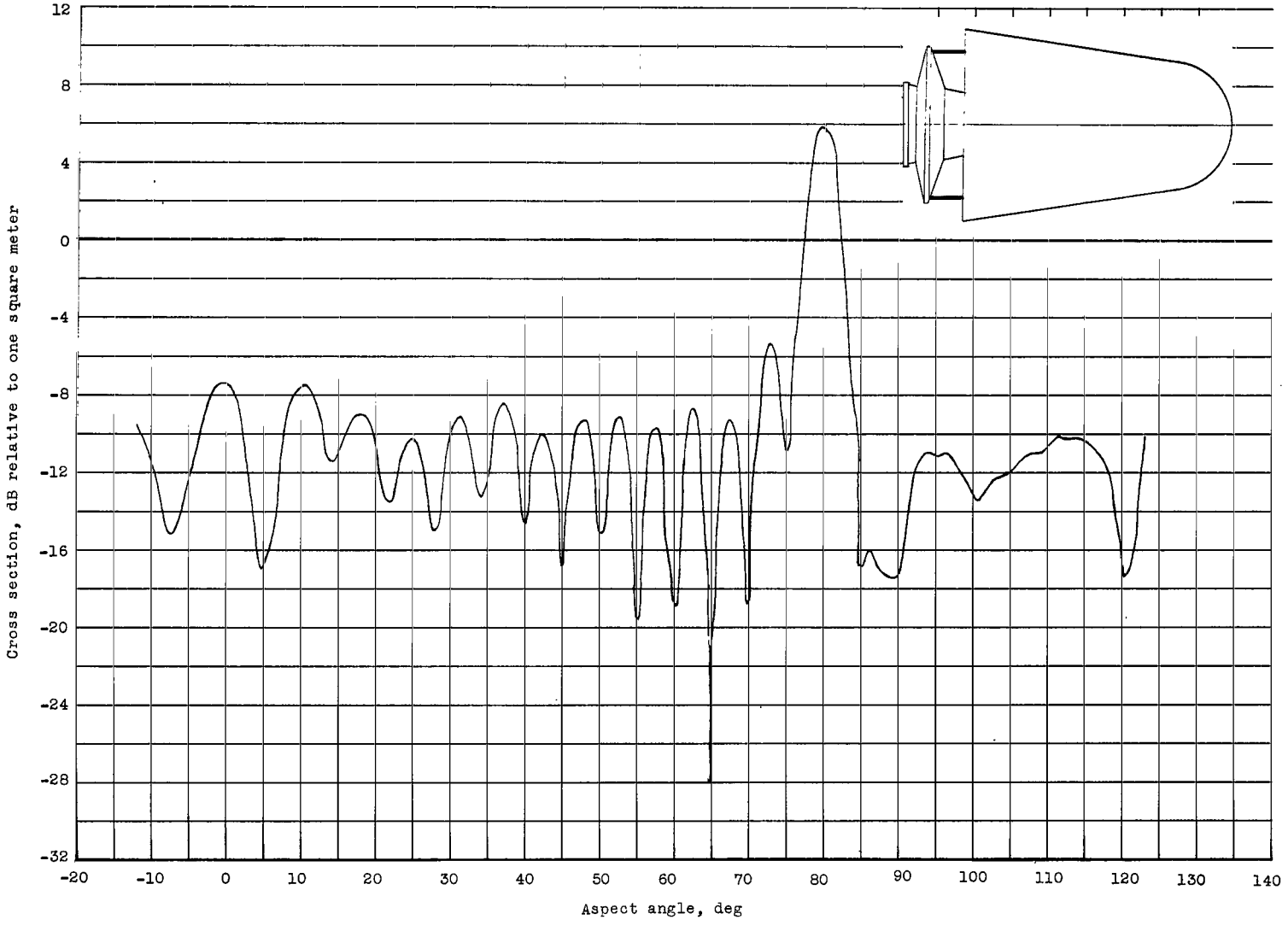

(b) Initial body position, roll 90° (antenna vertical); radar polarization, horizontal-horizontal.

Figure 16.- Continued.

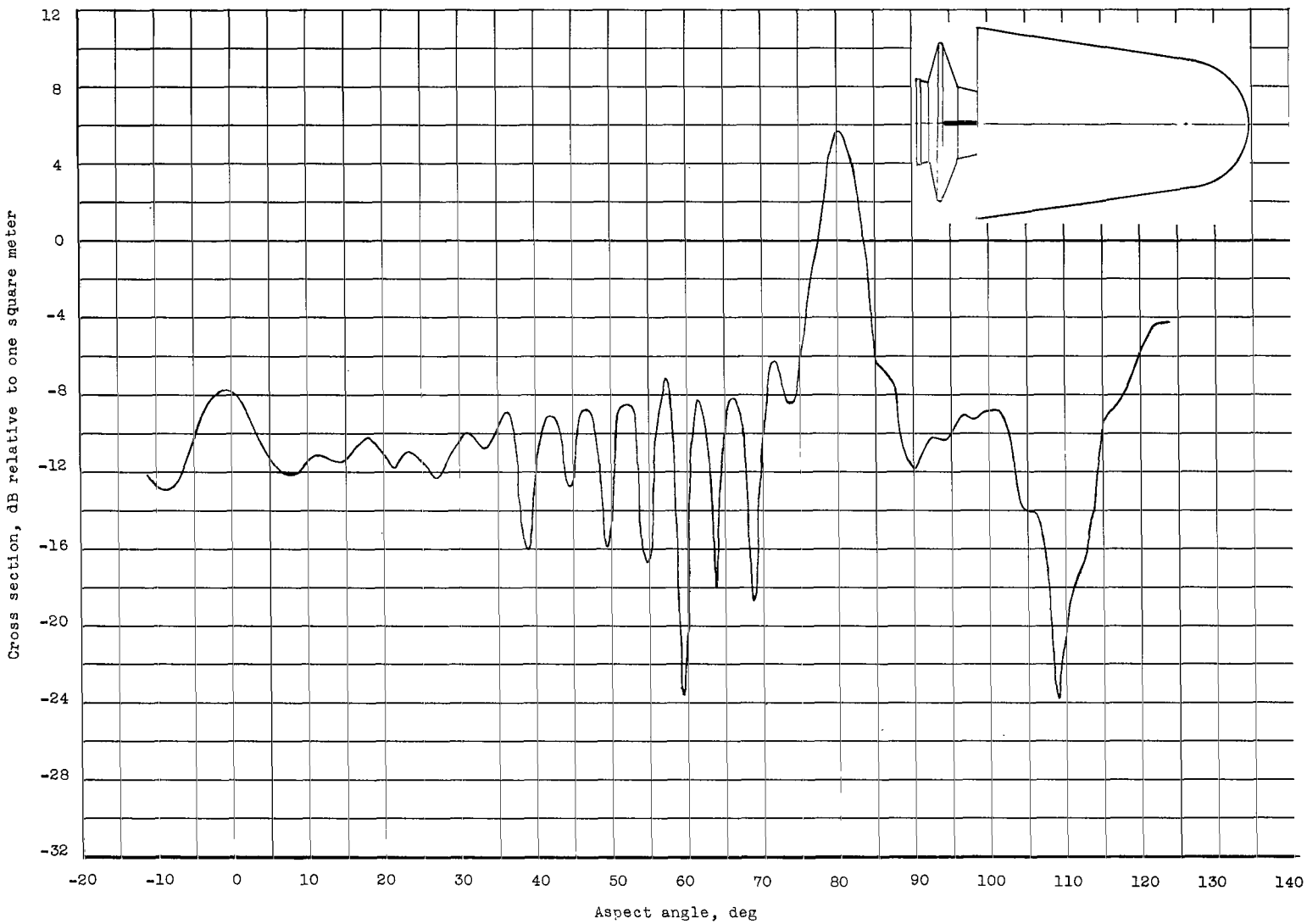

(c) Initial body position, roll 0° (antenna horizontal); radar polarization, vertical-vertical.

Figure 16.- Continued.

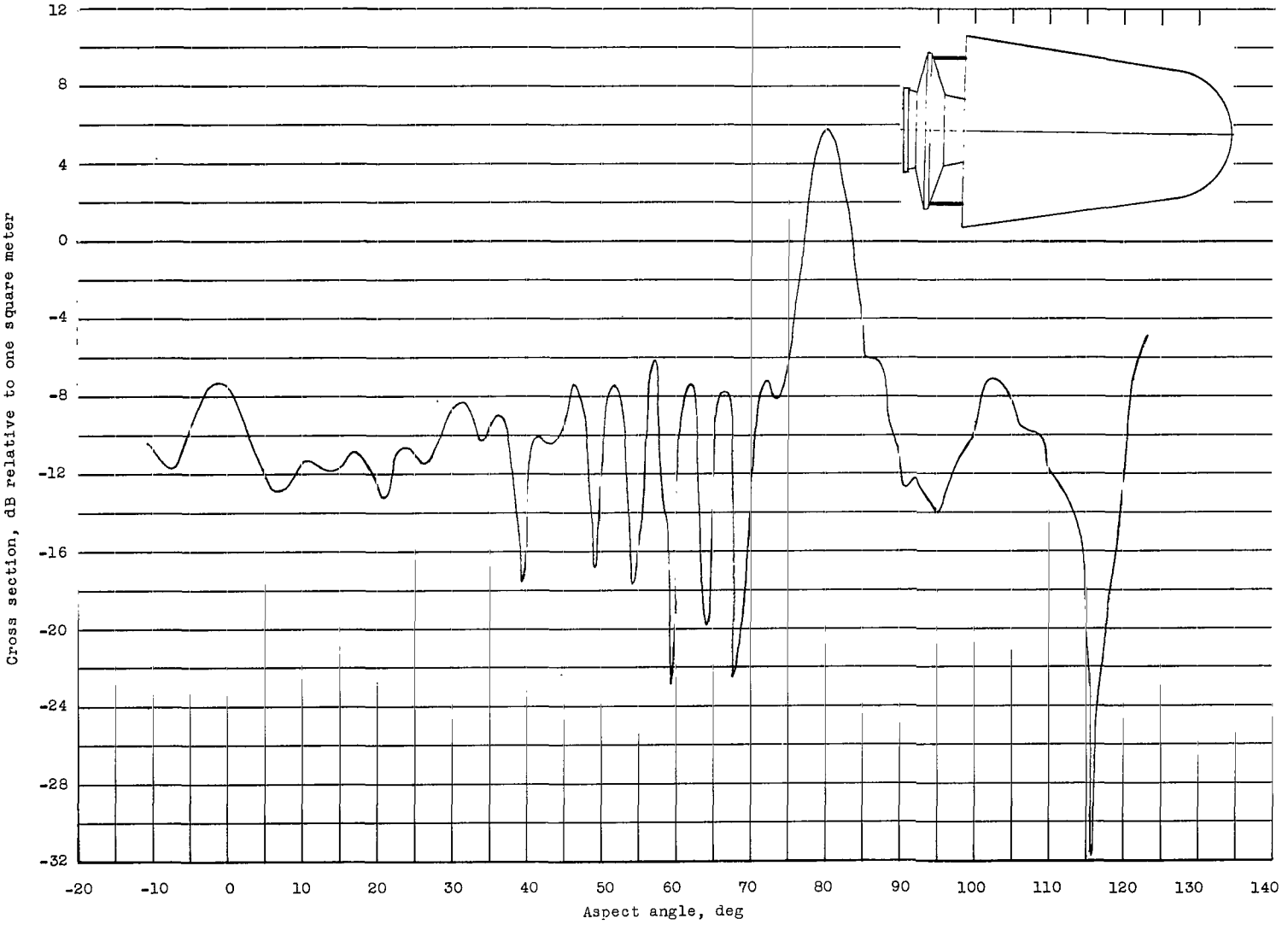

(d) Initial body position, roll 90° (antenna vertical); radar polarization, vertical-vertical.

Figure 16.- Concluded.

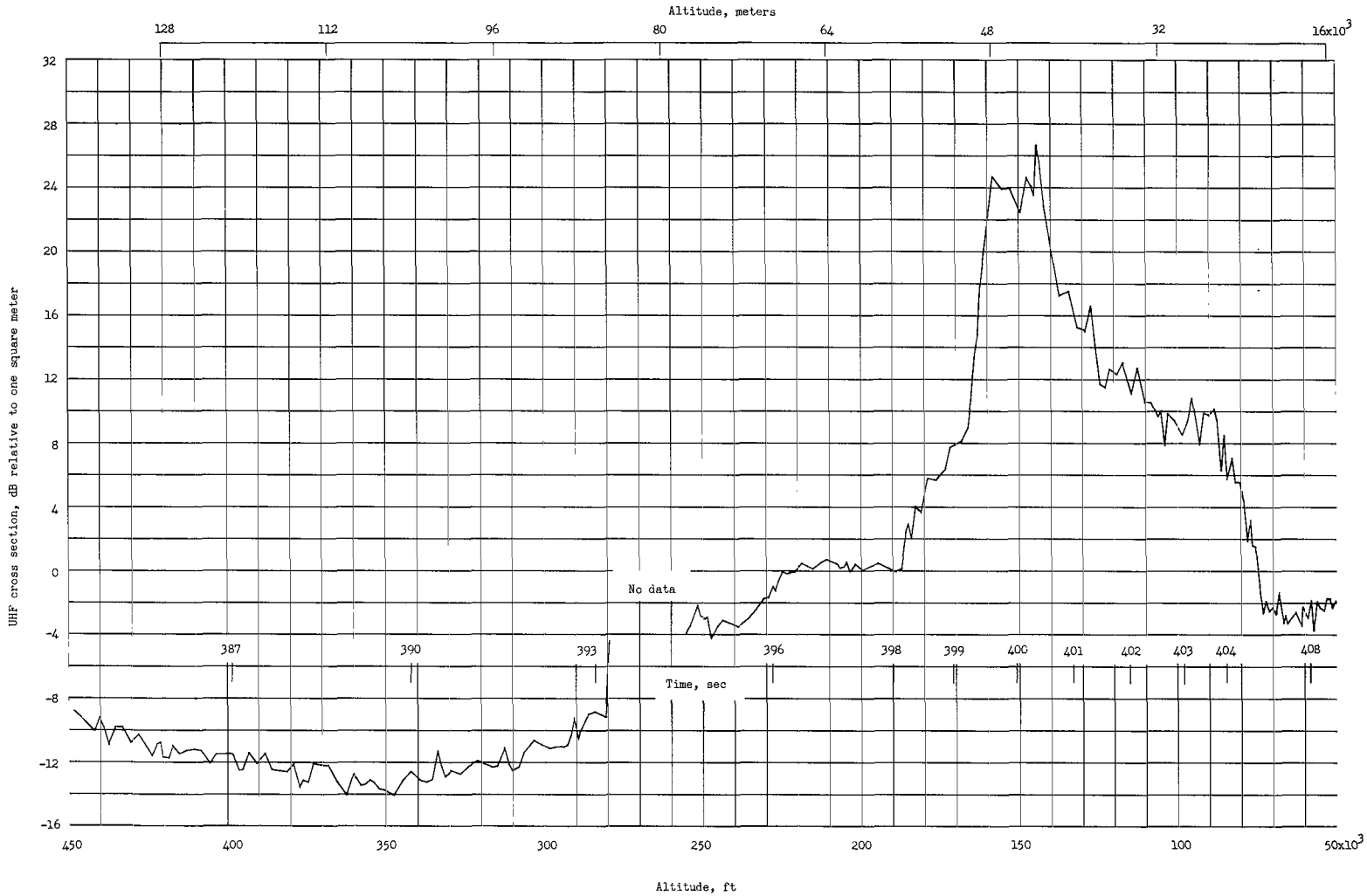

Figure 17.- Variation of UHF radar cross section with altitude for reentry of 9° cone.

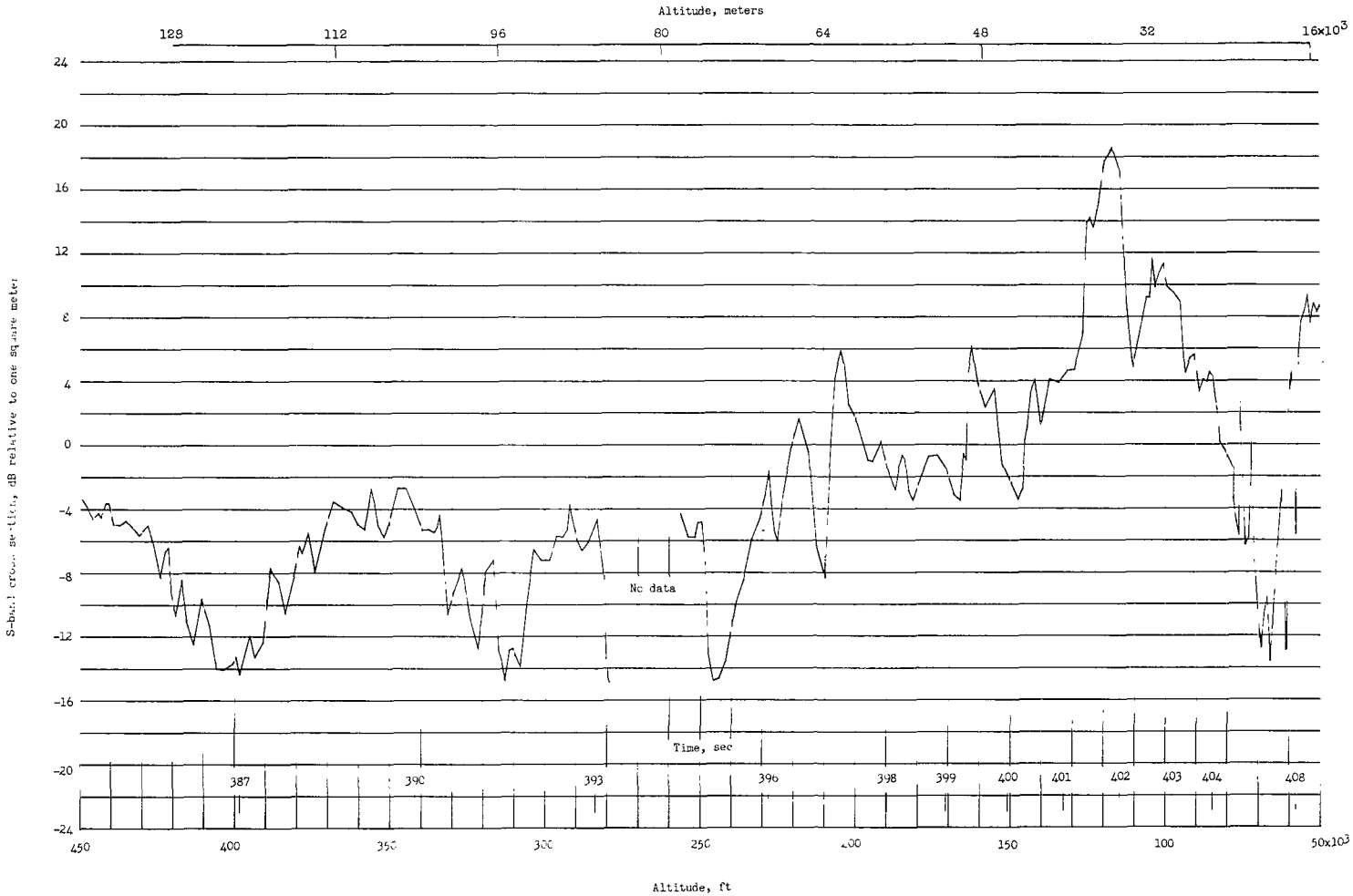

Figure 18.- Variation of S-band radar cross section with altitude for reentry of 9° cone.

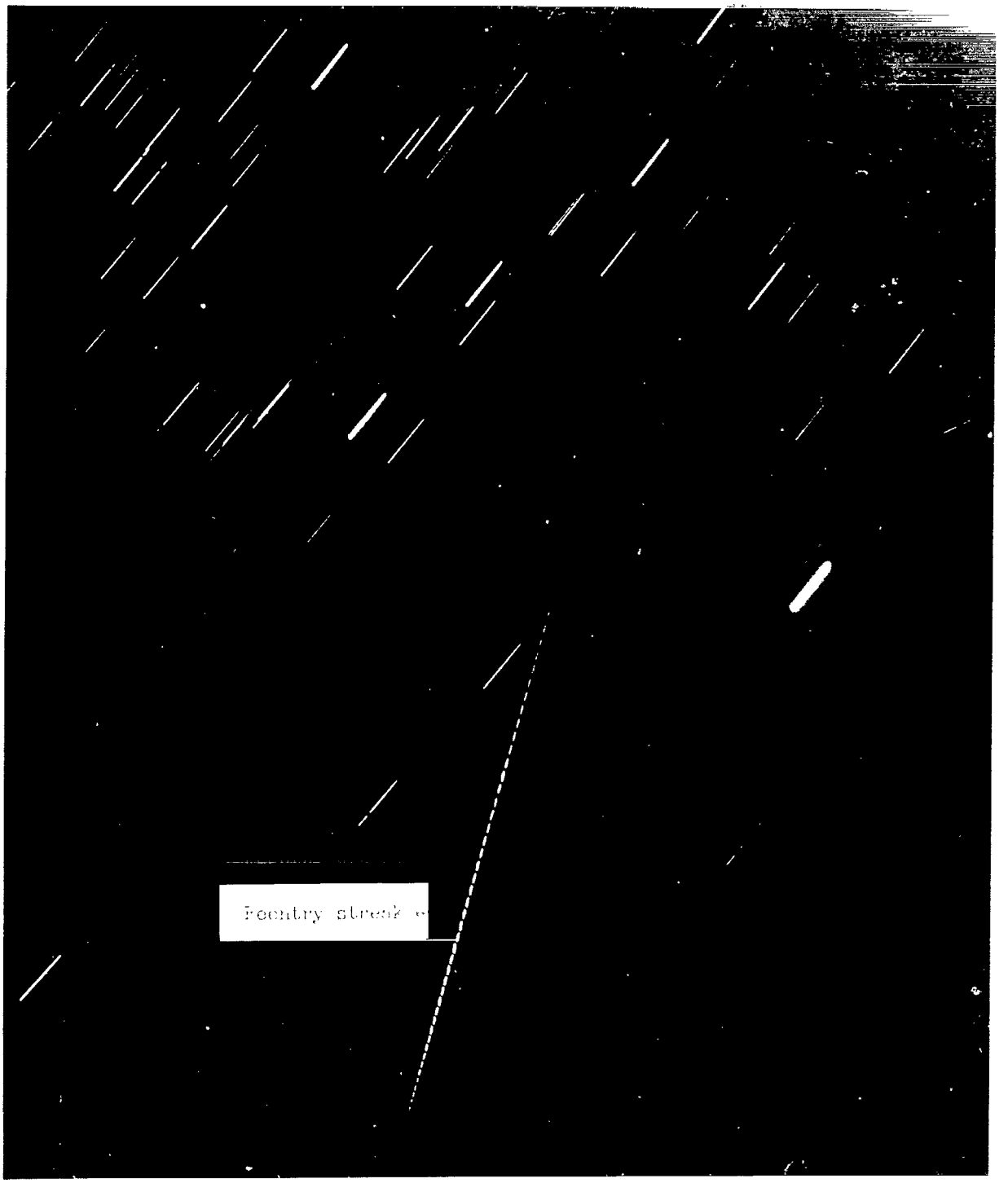

L-65-7931

Figure 19.- Time-exposed photograph showing optical reentry of 9° cone as seen from Coquina camera site and recorded on panchromatic film.

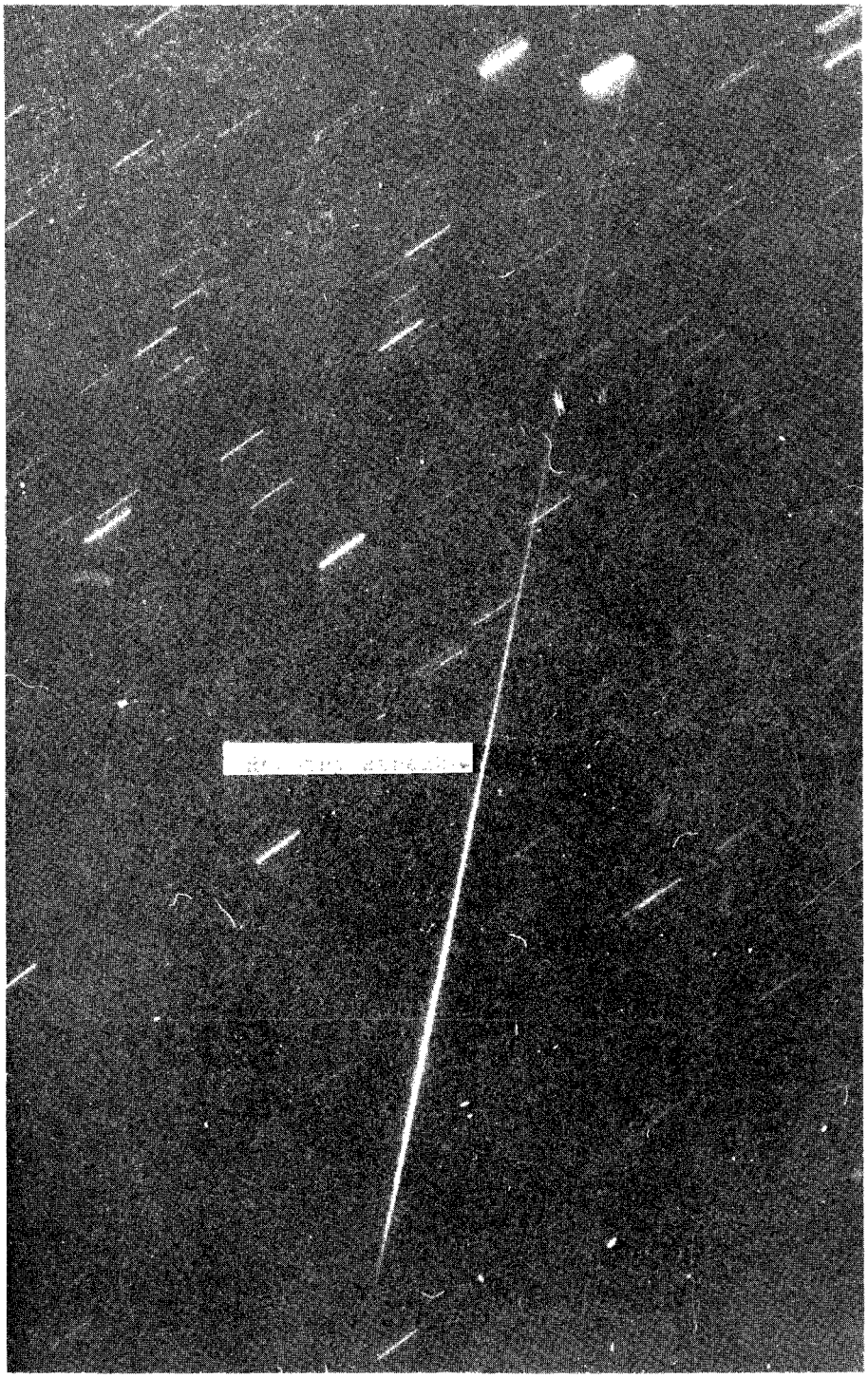

L-65-7932

Figure 20.- Time-exposed photograph showing optical reentry of 9° cone as seen from Wallops Spandar camera site and recorded on panchromatic film.

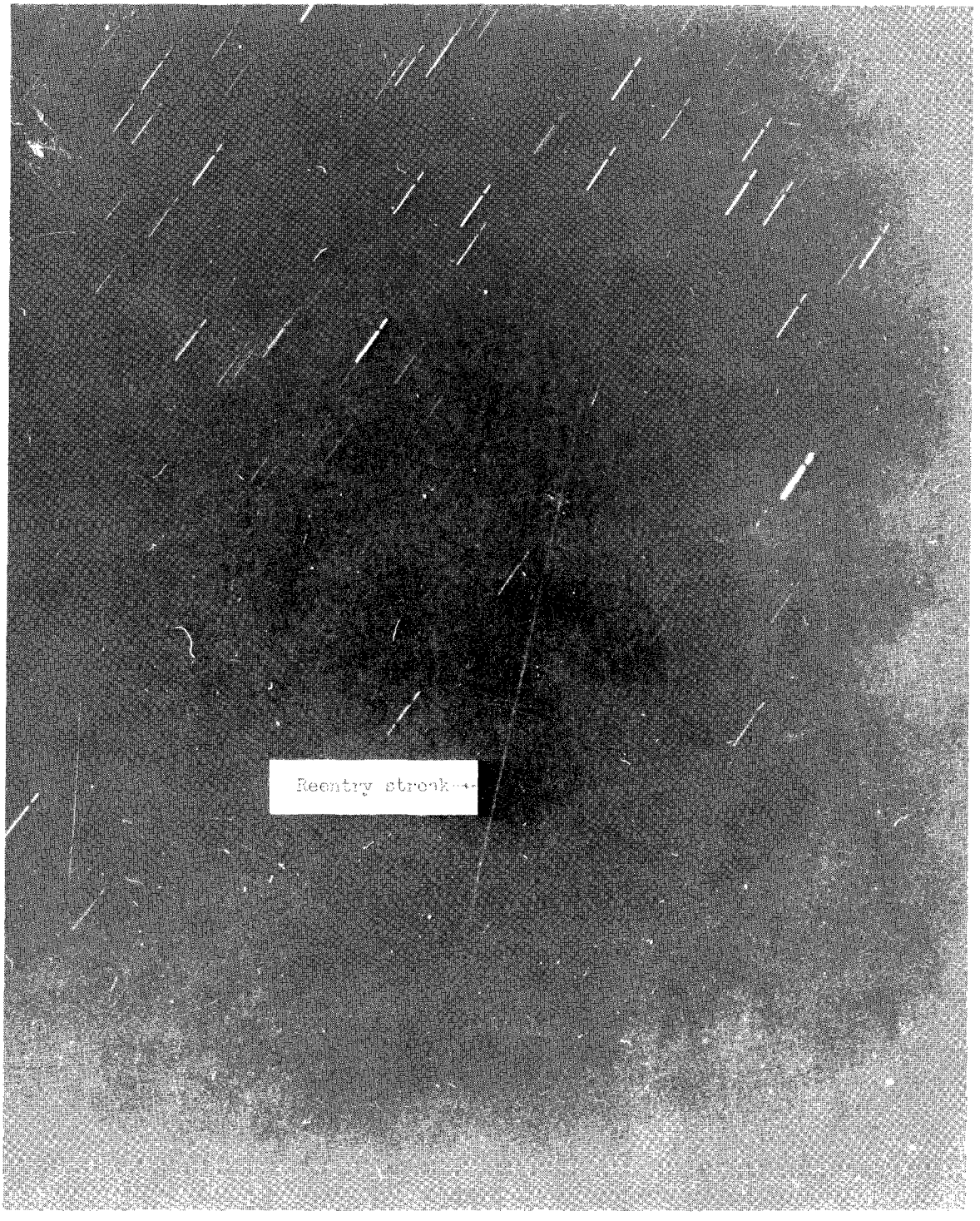

L-65-7933

Figure 21.- Time-exposed photograph showing optical reentry of 9° cone as seen from Coquina camera site and recorded on blue-sensitive film.

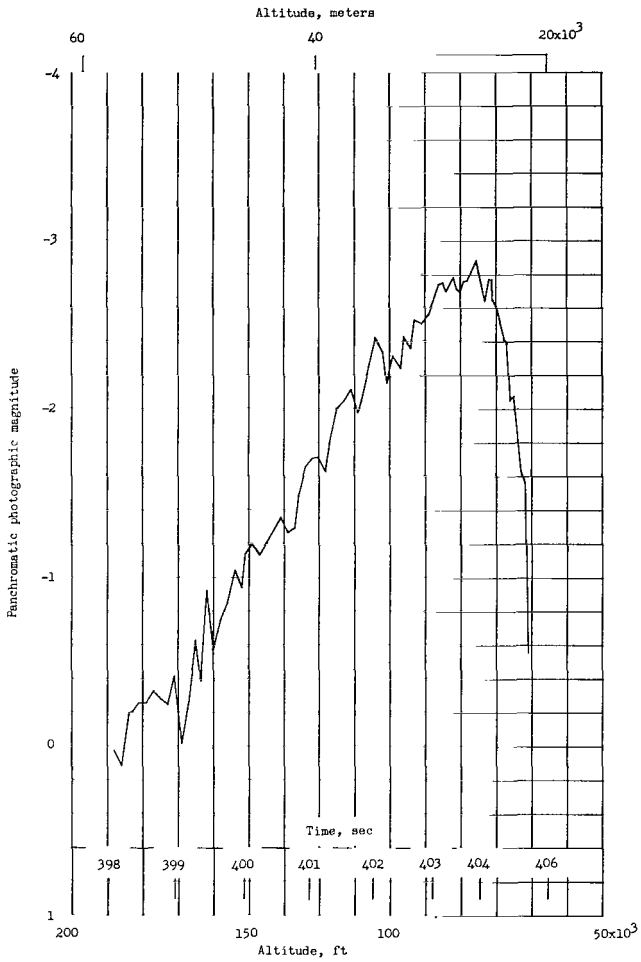

Figure 22.- Variation of photographic magnitude with altitude for 9° cone reentry as recorded by panchromatic film from Coquina site.

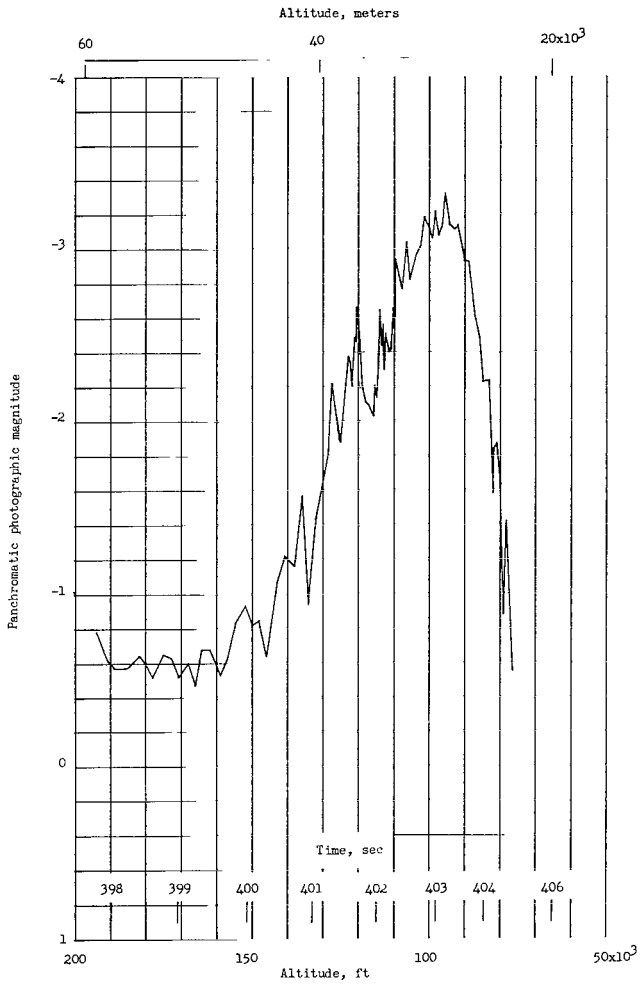

Figure 23.- Variation of photographic magnitude with altitude for 9^{o} cone reentry as recorded by panchromatic film from Wallops Spandar site.

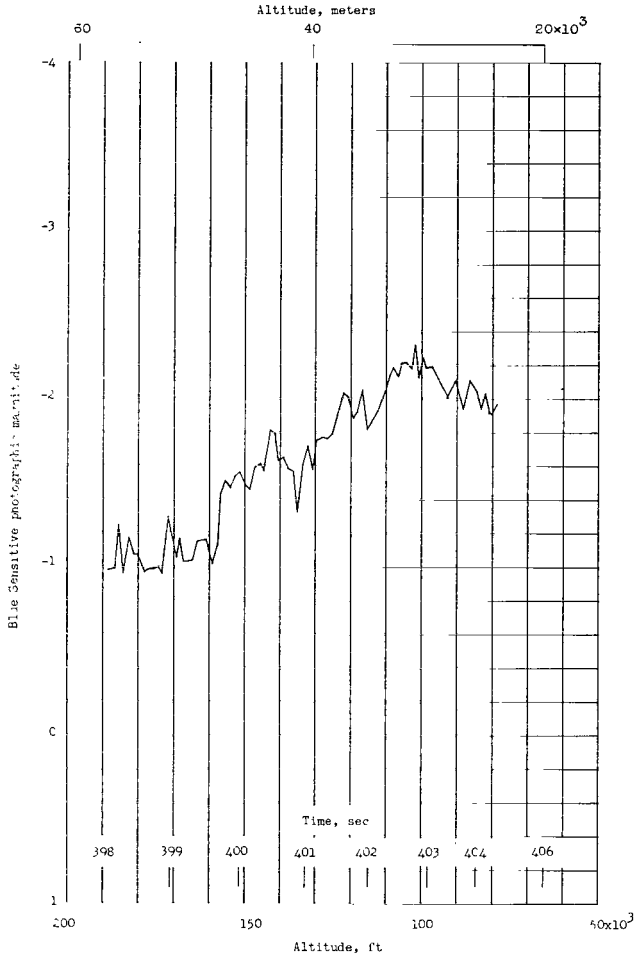

Figure 24.- Variation of photographic magnitude with altitude for 9° cone reentry as recorded by blue-sensitive film from Coquina site.

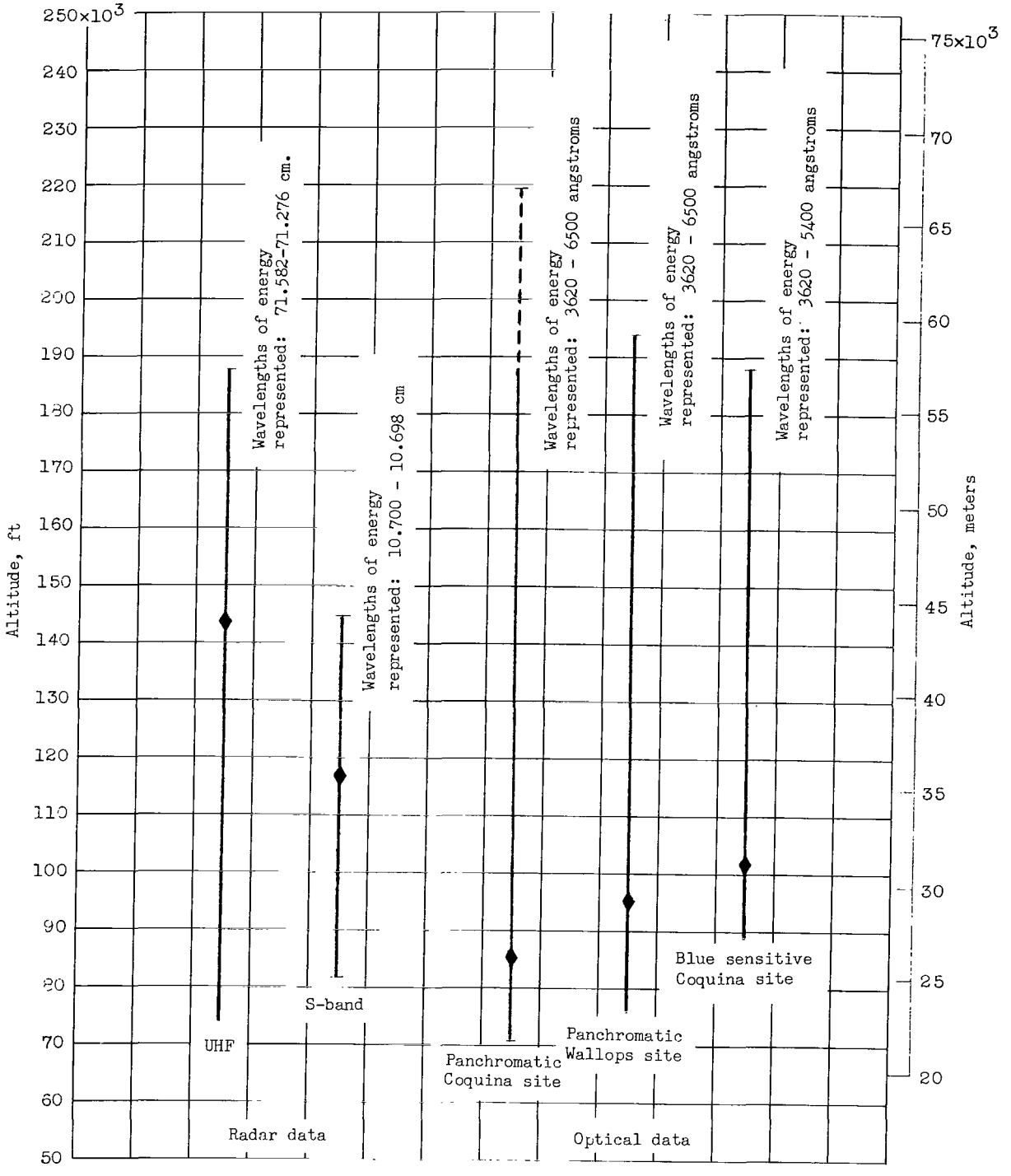

Figure 25.- Comparison of reentry data interval shown by radar and optical results from 9° half-angle cone. Diamonds indicate position of maximum values.

"The aeronautical and space activities of the United States shall be conducted so as to contribute . . . to the expansion of human knowledge of phenomena in the atmosphere and space. The Administration shall provide for the widest practicable and appropriate dissemination of information concerning its activities and the results thereof."

—NATIONAL AERONAUTICS AND SPACE ACT OF 1958

NASA SCIENTIFIC AND TECHNICAL PUBLICATIONS

TECHNICAL REPORTS: Scientific and technical information considered important, complete, and a lasting contribution to existing knowledge.

TECHNICAL NOTES: Information less broad in scope but nevertheless of importance as a contribution to existing knowledge.

TECHNICAL MEMORANDUMS: Information receiving limited distribution because of preliminary data, security classification, or other reasons.

CONTRACTOR REPORTS: Technical information generated in connection with a NASA contract or grant and released under NASA auspices.

TECHNICAL TRANSLATIONS: Information published in a foreign language considered to merit NASA distribution in English.

TECHNICAL REPRINTS: Information derived from NASA activities and initially published in the form of journal articles.

SPECIAL PUBLICATIONS: Information derived from or of value to NASA activities but not necessarily reporting the results of individual NASA-programmed scientific efforts. Publications include conference proceedings, monographs, data compilations, handbooks, sourcebooks, and special bibliographies.

Details on the availability of these publications may be obtained from:

SCIENTIFIC AND TECHNICAL INFORMATION DIVISION

NATIONAL AERONAUTICS AND SPACE ADMINISTRATION

Washington, D.C. 20546